MIGROGRID OPERATION AND CONTROL

by

Mohammad Saad Suleiman

A Thesis Presented to the Faculty of the
American University of Sharjah
College of Engineering
in Partial Fulfillment
of the Requirements
for the Degree of

Master of Science in
Electrical Engineering

Sharjah, United Arab Emirates

April 2021

Declaration of Authorship

I declare that this thesis is my own work and, to the best of my knowledge and belief, it does not contain material published or written by a third party, except where permission has been obtained and/or appropriately cited through full and accurate referencing.

Signature Mohammad Saad Suleiman

Date 10/05/2021

Approval Signatures

We, the undersigned, approve the Master's Thesis of Mohammad Saad Suleiman

Thesis Title: MICROGRID OPERATION AND CONTROL

Date of Defense: 22/04/2021

Name, Title and Affiliation	**Signature**
Dr. Ahmed Osman-Ahmed Professor, Department of Electrical Engineering Thesis Advisor	
Dr. Amr Mohamed El Nady Associate Professor, Department of Electrical Engineering, University of Sharjah Thesis Co-Advisor	
Dr. Mostafa Farouk Shaaban Associate Professor, Department of Electrical Engineering Thesis Committee Member	
Dr. Raouf Fareh Associate Professor, Department of Electrical Engineering, University of Sharjah Thesis Committee Member	
Dr. Nasser Qaddoumi Head Department of Electrical Engineering Program	
Dr. Lotfi Romdhane Associate Dean for Graduate Affairs and Research College of Engineering	
Dr. Sameer Al- Asheh Interim Dean College of Engineering	
Dr. Mohamed El-Tarhuni Vice Provost for Graduate Studies Office of Graduate Studies	

Acknowledgements

First, I would like to thank God for the blessing of patience and energy needed to end this thesis. I would like to express my thanks to my family, whose words are not enough to express my gratitude to them, for their endless support and their prayers for success for me.

I want to thank my advisors Prof. Ahmed Osman and Dr. Amr Elnady for their continuous guidance and patience especially with the various problems we faced to accomplish this work. They were always there for me welcoming discussions and suggestions.

I would like to express my sincerest gratitude to the American University of Sharjah (AUS) for the financial support I received through graduate assistantship and for the great experience I gained during my Master program studies. Furthermore, I would like to extend this appreciation to all the professors at AUS with whom I attended graduate courses.

Special thanks to Saif Sinan and Sadique hamdan for their assistance during my thesis.

Finally, I'd like to express my gratitude to all of my AUS friends and colleagues for their time and support.

Abstract

The world is moving toward renewable energy resources as a result of rising energy demand and the decline of fossil fuels. This move led to the shift of interest from the centralized conventional electric grids to decentralized smart grids. Microgrid is the basic structural unit of smart grid, it can utilize both renewable and non-renewable types of distributed generator (DG) technology. As many renewable DG technologies and storage elements are based on DC power, while many loads and devices depend on AC power, the importance of inverter-based DG technology increased. The output of these inverters in an islanded microgrid must achieve a good current sharing between DG unites in microgrid, maintaining stability and synchronization between DGs, and keeping voltages and frequencies within specific range. These criteria can be achieved with various control strategies including centralized control, master slave control, current distribution control and droop control methods. Consequently, the control and operation of microgrid is a challenging task that requires overcoming the obstacles relates to the nonlinearities and disturbances in the power system. In this thesis work, two feedback control strategies were developed and implemented in droop control to operate multiple DG units in a microgrid. The two control strategies are state feedback control and hyperbolic tangent exponential Sliding Mode Control (SMC). The developed state feedback control provided a powerful performance with respect power sharing accuracy in steady state conditions and regulating the voltage and current disturbance caused by other DG units within the same microgrid. The proposed hyperbolic tangent exponential SMC utilizes the exponential SMC method and hyperbolic tangent reaching mode to provide robust, accurate, reliable behavior against unmodeled dynamics, hard nonlinearities, and parametric uncertainties. Furthermore, an experimental set is built to imitate a microgrid operation in real life application.

Keywords: ***Microgrid; droop control; distributed generation, multi-level inverter, sliding mode control, state feedback control***

Table of Contents

List of Figures

List of Tables

List of Abbreviations

DER	Distributed energy resources
DG	Distributed generator
PCC	Point of common coupling
POI	Point of interconnection
SMC	Sliding mode control

Chapter 1: Introduction

This chapter introduces different control methods of distributed generators (DGs) in microgrids, and the encountered problems by these methods are presented. Then, the selected control method and the problem in this study, and the proposed contribution of this thesis. Finally, the general organization of the thesis will be presented.

1.1. Background

Recently there has been a significant improvement in generating renewable energy through distributed generation concept. Distributed generator (DG) is a small-scale generator that can be connected near or far from the loads. This technological development increases the interest and needs to connect an individual or multiple DG units to the main grid to operate the DG unit in grid-connected mode. Moreover, the DG units can be connected off the grid to supply local loads forming what is known by a stand-alone micro-grid. Connecting multiple DGs in parallel is considered a challenging task. That complexity is related to circulating current caused by the phase's differences and the generated voltages' magnitude. In ideal cases, this can be solved by placing an impedance at the output of each DG [1]. In contrast, real-life systems are far from ideal. As choosing the type and the value of the output impedance is considered a challenge on its own. Another problem can be caused by deference in the parameters of each DG and its output impedance. This deference leads to inequality of power-sharing between DGs [2]. Several control schemes were used to overcome these problems; these schemes can be categorized into two categories [3]:

- Communication-based schemes such as: centralized control, master/slave control, current sharing controls, and angle droop control.
- Non-communication schemes such as: droop control and its variations.

1.2. Problem statement

In an islanded microgrid a good current sharing and maintaining stability between DG unites must be achieved, as well as keeping voltages and frequencies within specific range. The control and operation of microgrid is a challenging task that re-

quires overcoming the obstacles relates to the nonlinearities and disturbances in the power system.

Having an experimental setup is an essential requirement to study the real-life challenges in operating microgrids.

1.3. Thesis Objectives

This thesis focuses on designing 3-phase droop control to enhance power-sharing and stability of the system using different feedback control strategies in the voltage and current loops.

The second objective is to build an experimental setup that represents a microgrid considering all its elements. The purpose of building this experimental microgrid set to imitate a microgrid operation in real life application. Therefor, to be able to study and resolve practical challenges in power system.

1.4. Research Contribution

The contributions of this research work are in two areas, the feedback controllers used in droop control inner and outer loops and the structure of the practical microgrid used in the thesis. These contributions are:

- Design and application of hyperbolic tangent exponential sliding mode control (SMC) in current loops of droop control to achieve accurate power sharing along with suppressed chattering.
- Design and application of state feedback control to serve as both voltage and current loops in droop control to achieve accurate power sharing between DGs in the microgrid.
- Build an experimental setup that represents a microgrid considering all its elements to imitate a microgrid operation in real life application to be able to study and resolve practical challenges in power system.

1.5. Organization

The following is how the rest of the thesis is organized: Chapter 2 provides background about microgrid, types, problems in microgrids, and solutions. Moreover,

related works to this research are discussed. The employed methods and algorithms are discussed in Chapter 3, along with the implementation of the proposed structure. Chapter 4 presents the performance evaluation for the employed streaming and allocation algorithms using simulation results. Chapter 5 shows the practical implementation on the microgrid in this study. Chapter 6 evaluates the setup and provides preliminary practical results using the built setup. Finally, Chapter 7 concludes the thesis and outlines its future work.

Chapter 2: Literature Review

2.1. Introduction

This chapter gives an overview about microgrids and its types, then discusses the technical problems of microgrids. Moreover, the review shows power control schemes used to regulate microgrid issues. Additionally, feedback controllers in droop control used by researchers are also discussed. Finally, a brief review about inverter types is presented.

2.2. Microgrid

Any group of electric loads and DGs with defined electrical limitations that work as a single controllable unit in both grid-connected and islanded modes is considered microgrid [4]. Based on this definition, the microgrid structure can be represented by multiple DGs connected in parallel together, such as photovoltaic systems, electrical storages, wind turbines and/ or generators, and different types of loads as shown in Figure 2.1. Microgrid structure may contain different kinds of storage elements such as battery systems, flywheels, and super-capacitors. Such storage elements can work as backup energy supplies in case of higher load demand than the source's capability or work as a load when the load demand is low. This change in the operation of storage elements can stabilize the microgrid against a sudden load change [5]. The amount of DGs in microgrid is only limited by the number of possible energy resources, as one of the microgrid's objectives is to utilize the surrounding energy resources to achieve higher efficiency and reliability.

2.2.1. Microgrid modes. Microgrids can be categorized based on its operational mode, whether connected to the grid (grid-connected mode) or disconnected from it (islanded mode). The islanded mode can happen due to either unplanned Islanding (like emergency in hospitals) or planned islanding. This is case where the microgrid works in standalone mode and has the objective to generate the loads' needs of active and reactive power of the load connected to it, while maintaining the voltage and the frequency within certain range. While in the grid-connected operation, it is required from

the microgrid to inject active and reactive power to the utility grid while having the ability to supply the local load connected to it [6]. The connection between microgrid and power grid can be seen in Figure 2.1, where the switch at the point of interconnection (POI) is responsible for changing microgrid's operation from grid-connected mode to islanded mode.

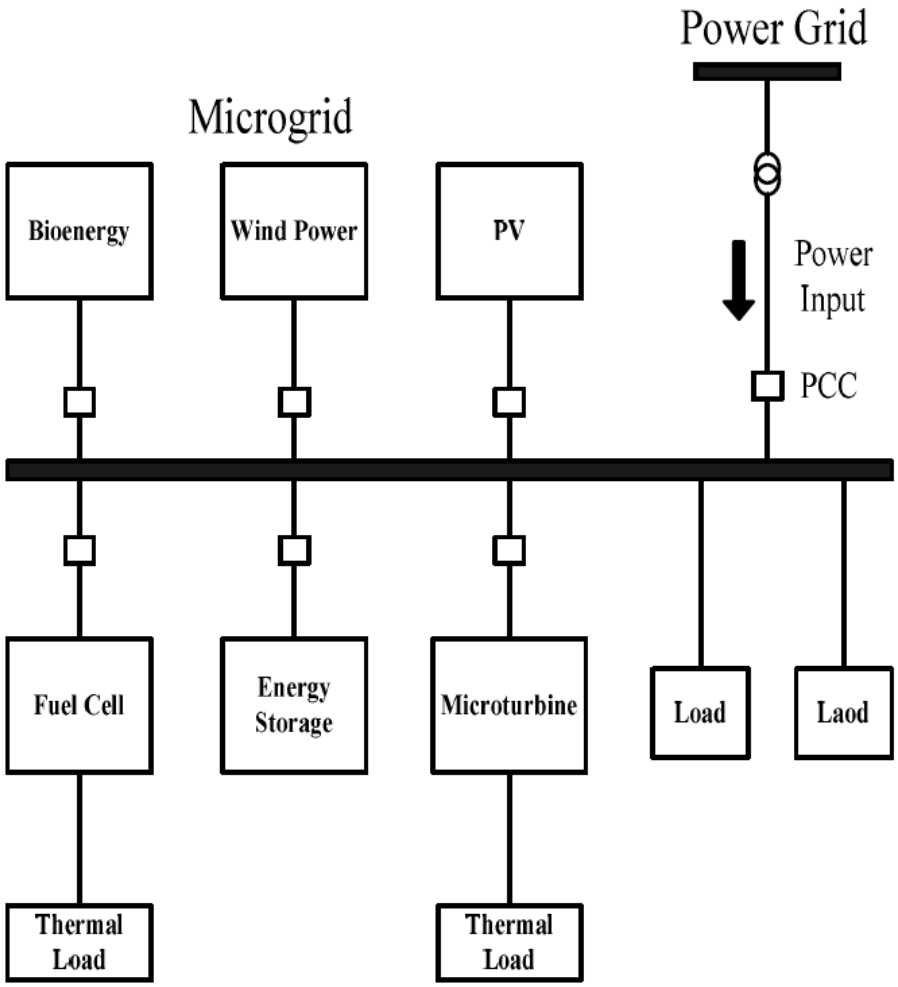

Figure 2.1: Microgrid with multiple DGs, loads and storage elements [7].

2.2.2. Technical problems in microgrid. Technical problems in microgrid can be divided into two categories based on the mode of operation, grid-connected or islanded mode, and can be seen in the areas of power quality, voltage stability, harmonics, reliability, protection, power sharing and control [8].

Electric power quality in AC microgrid can be defined as Maintaining the sinusoidal shape of the voltage at rated magnitude and frequency. In grid-connected mode,

the voltage shape and frequency are mainly following the voltage at the POI in the grid, and it is supported mainly by the grid and the effect if the microgrid is minimal. There is no support from the grid in islanded mode, and microgrid completely controls the voltage shape, and frequency [9].

Voltage stability is maintaining the voltage magnitude, angle, and frequency osculation within lower limits of change. These changes happen in microgrid in case of disconnecting it from the main grid, connecting or disconnecting DG from microgrid, or applying MPPT at inverters connected to microgrid.

The harmonics occur in microgrid when power electronic converters are used, as the switching frequencies of MOSFET/ IGBT converters will cause current components with higher frequencies than the power frequency to happen. Hence, the power loss will increase. Moreover, the harmonics may damage other components in the microgrid. To solve this issue, a power lowpass filter should be added to the output of the converters. The size of the filter depends mainly on the switching frequency; as we increase the frequency, the harmonics will decrease; therefore, the size of the filter will decrease [10].

The control of microgrid is divided into three levels, primary, secondary, tertiary control levels. The primary level is considered component level control as it is responsible for maintaining the microgrid stability and applying load sharing between DGs in microgrid, as one of microgrid's objectives is to utilize the energy sources where the microgrid is installed as much as possible. Hence, it is logical to have more than one DG connected to the microgrid. The primary level is also responsible for the output voltage and frequency of DGs.

Secondary control level is microgrid control level as the objective of this level is to control the POI in microgrid. This level is built with simple commands such as: connect DG to the microgrid or disconnect, make sure that the net power at POI is equal to zero and apply protection techniques. Tertiary control main objective is connecting the microgrid to the main grid or disconnect it [3].

As the interest of this thesis is the operation of microgrid in an islanded mode, and tertiary control level is not needed. The focus will be on using and applying primary and secondary controls to improve the operation of microgrid in an islanded mode.

Several control methods were applied on microgrid to achieve stability, reduced harmonics, load, and harmonics sharing, such as centralized control, master-slave control, Distributed current Control, and droop controls.

2.3. Control Techniques in Microgrid

The control techniques used in microgrid can be classified as communication and communication-less techniques. The centralized control, master-slave control, distributed current control, and angle droop control are categorized under control techniques with communication, and frequency droop with its variations are considered as communication-less methods.

2.3.1. Centralized control. In this control technique, a controller is placed at the POI. The main objective of this control is voltage stability and to keep the active and reactive power shared between all the DGs in the microgrid by controlling their output current, hence a communication link is needed between every DG and the controller at the POI. The structure of the centralized control can be seen in Figure 2.2.

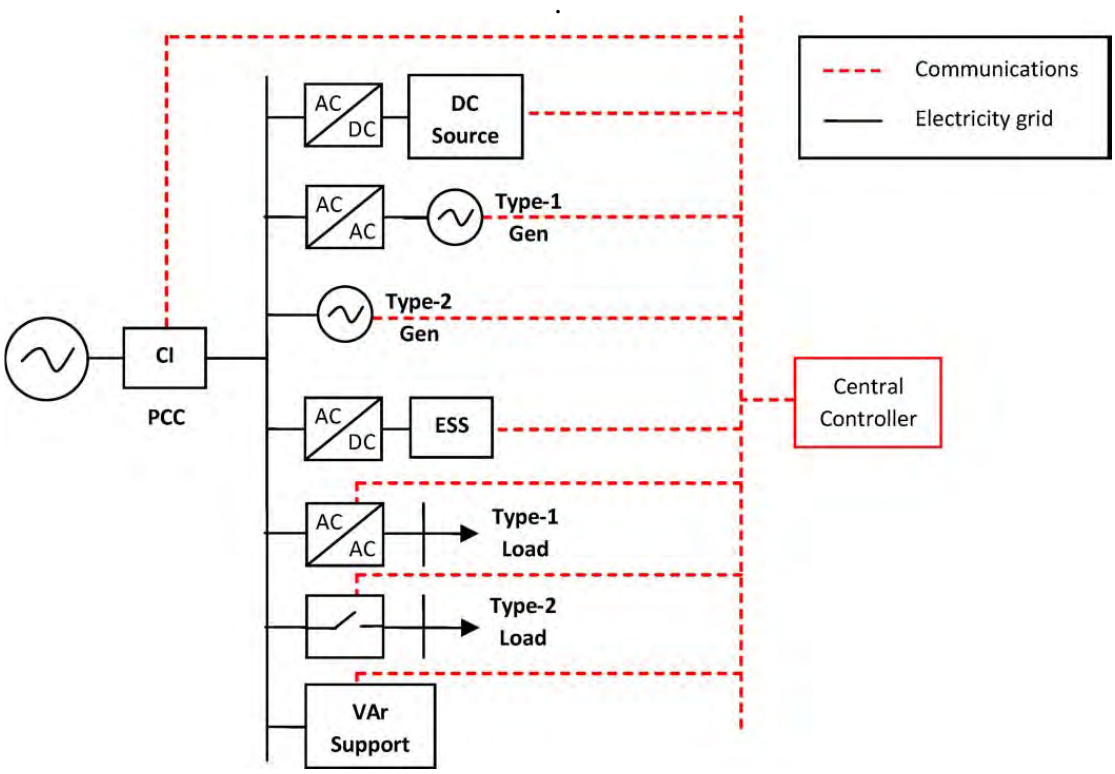

Figure 2.2: Centralized control microgrid structure [3].

A centralized controller has a huge advantage in achieving the accurate and equal current sharing between DGs in the same microgrid [11]. The single point of failure is considered as the main disadvantage of this method, as the functionality of the controller depends on the functionality of every module of the system [4]. Another disadvantage is the requirement of a high bandwidth communication channel between every DG and the controller at POI [12].

2.3.2. Master-slave control. In this control method, one of the DG units will act as a master voltage source that will support the system voltage to the whole system. The other units will function as slave current sources to follow the power reference that is provided by the master unit [13]. A good example can be provided for the PV-storage-based microgrid where the storage acts as a voltage control source in addition to the frequency, and the PVs are the slave current source units. A good representation of master-slave control can be shown in Figure 2.3.

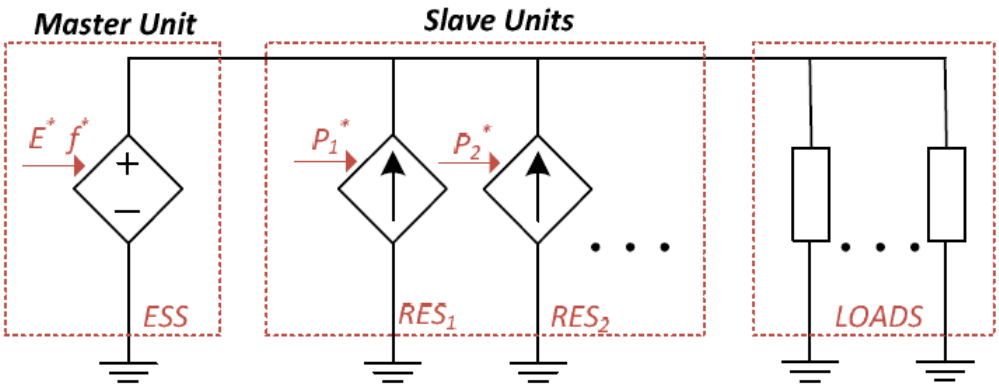

Figure 2.3: Master-slave control for islanded microgrid [14].

In master-slave control, slave control units cannot independently operate as if they need the master source to respond properly. In addition to that, they cannot react to the variations happened by the load power. This is a main drawback issue of the master-slave control method [15]. However, this method's good power management encourages researchers to use it in their work and improve its functionality. In [16], They used the master-slave control strategy. They enhanced it by resolving the phase

difference between the master and slave by using a controller for phase synchronization. They ensured that constant output voltage would be provided even during the master unit failure. Others proposed a hybrid master-slave and droop control to give a better control method where they could make the control that has a low resistive line impedance and power-sharing and reliability [15].

2.3.3. Distributed current control. A distributed current control strategy must only be used with balanced power systems. The output voltage is controlled using the average required current by the loads [4]. To achieve current sharing, the controller will get the average current by measuring the total load current and divide it by the number of DGs of the system as illustrated in Figure 2.4.

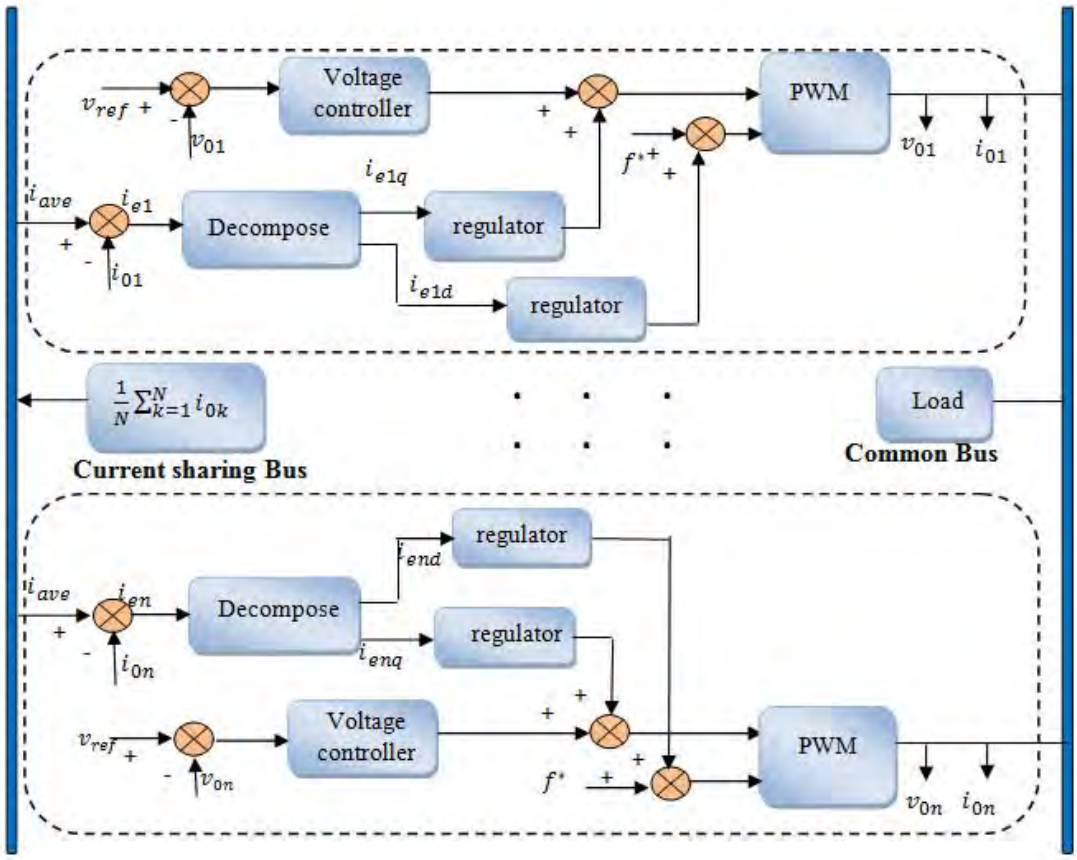

Figure 2.4: Control structure of the distributed control [4].

The figure discuss the structure of the distributed control system. The current sharing bus is responsible for calculating the average current required so that each DG

will use it to generate the output current equal to that average regardless of the DG limitations [17]. The advantages of the current sharing are that it has a good transient response, and it also minimizes the circulating currents between DGs. This method's main disadvantages are the need for low bandwidth communication links and the ability to work with unbalanced systems.

2.3.4. Droop control. All previously mentioned methods require installing a communication link either between DGs or from DGs to the central controller. Adding such a communication link will increase the installation cost and lessen the systems' ability to grow [18]. To overcome such issue, a communication-less approach must be taken. Droop control works similarly to a synchronous generator. When the input mechanical power is less than the output ac electrical power, the inertia of the generator will reduce the rotational speed. Thus, the frequency of the output [19]. This action will change the power angle, which will lead to the reduction of the output power. The structure of the system shown in Figure 2.5 is used to achieve such behavior. One of the main advantages of this structure is its flexibility as it can easily work as plug and play control method, and it does not need any communication between DGs. Disadvantages of droop control in microgrid droop control was widely accepted since it is a communication-less control method, which makes it a plug-and-play control [4]. Still, it has several disadvantages that affects its applicability Such as:

- Poor dynamic performance.
- Poor harmonics sharing.
- Power sharing is affected by inequality on line impedance of each inverter.
- Weak in regulating voltage.

Droop control in islanded microgrid has recently attracted researchers since it is easy to be used with the conditional grid. Researchers' works were focused on improving and modifying the droop control to bypass its weaknesses. The modifications can be categorized as follows, Virtual impedance loop-based droop control, adaptive droop, power angle droop, and reverse droop. [4] [20].

2.3.4.1. *Virtual impedance loop-based droop control.* Adding a proper virtual impedance to the voltage and current feedback loops results in improving the reactive

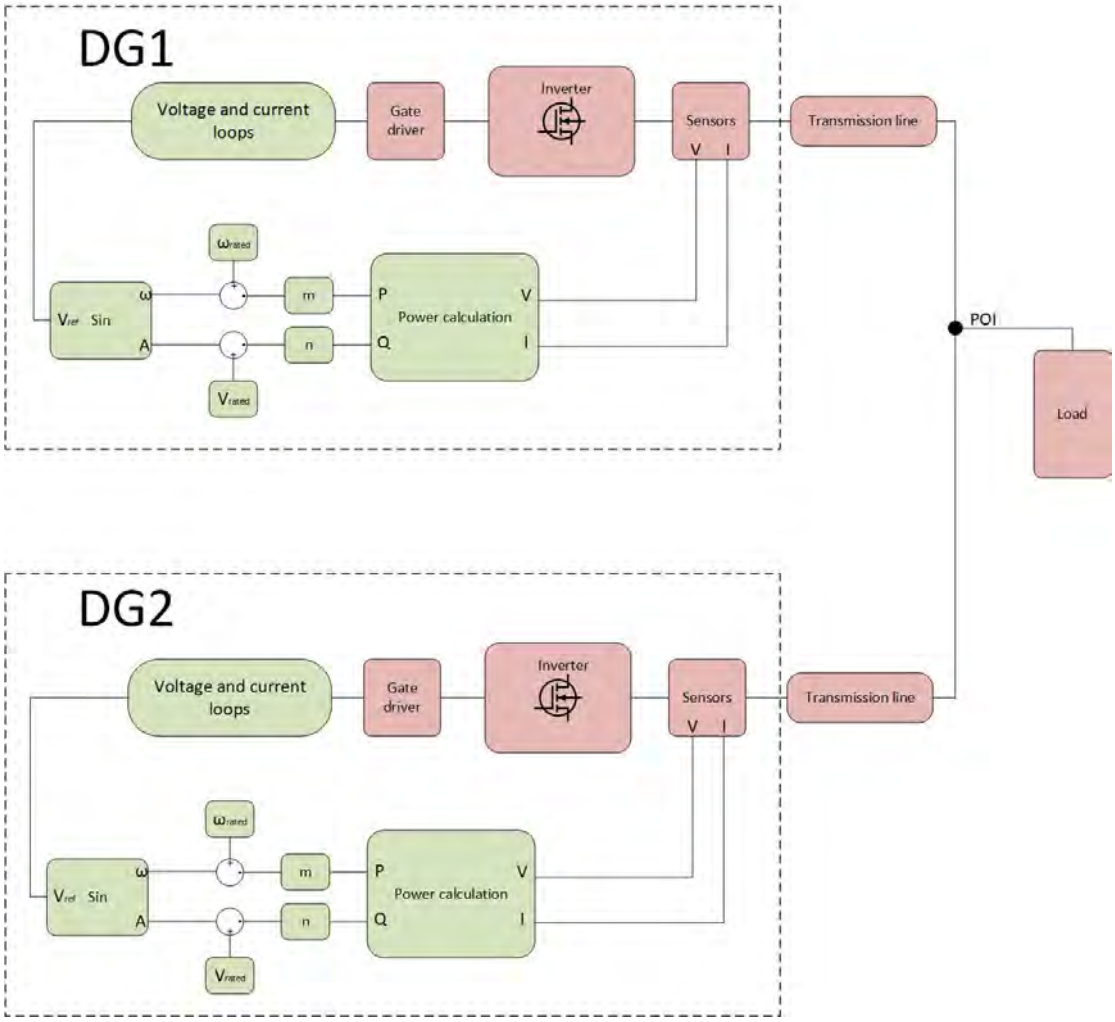

Figure 2.5: Single phase microgrid based on droop control scheme.

power sharing between inverters in the microgrid. The virtual impedance is used as a multiplier to the output current, which will be used as part of the voltage control loop's reference voltage.

Selecting the virtual impedance is the main problem of this method, as it is not easy to get the exact values of line impedance for each DG. Some cases like [21], the value of this virtual impedance is selected to dominate the line impedance to bypass the effect of voltage regulation across the line, therefore improving the power-sharing. In [21], the author used a complex virtual impedance to achieve accurate proportional load sharing in medium voltage microgrid. The introduced complex virtual impedance improved voltage/reactive power V-Q control, eliminating reactive power sharing errors due to imbalanced line impedance. [22] presented a way to design and implement

a virtual impedance for power electronics DGs. It also developed a flexible small signal microgrids model with different operation conditions: this improved system stability and reduced power couplings. Based on the developed microgrid models, the DG impedance range was selected to achieve stability, improved transient response, and power flow performance. In [23], improved droop control is introduced by using a 1st order RL high pass as virtual output impedance, which also added an integral-derivative term to the conventional droop technique. This controller improved the transient response and active and reactive power-sharing. Selecting PID parameters and filter parameters is considered the main disadvantage of this method.

Virtual impedance Droop control is also used in [24] to improve THD sharing between inverters. The authors introduced a negative Virtual Harmonic Impedance to achieve the THD sharing between different ratings DGs. The authors also managed to develop a method to estimate the required impedance value for THD sharing, which allowed the virtual impedance to adapt based on the needs. The results showed a good harmonic sharing between the inverters once the impedance is added. [25] used communication link between DGs to calculate the required virtual impedance to get perfect reactive power-sharing. Their method requires the measurement only once the system is activated, then the communication link is not needed afterward. The main benefit of this method is that it does not require knowledge of the feeder impedances. Therefore, it is easy to be implemented on any system. The main disadvantage in taking away one of the most desired features in droop control is even for a short amount of time.

2.3.4.2. ***Adaptive droop control.*** One of the problems of conventional Droop control is that it has a slow transient response, and it has inaccurate power-sharing compared to other controls, as the control scheme does not accurately follow the actual physical characteristics of the microgrid [26]. One good advantage of the adaptive droop control is that it does not require detailed knowledge about the control of the system where the control parameters will be self-adapted to achieve optimal performance.

In this technique, the maximum reactive power Q_{max} drawn from each unit is compared with a reference value of reactive power Q_{ref}. If the Q_{max} is more than the Q_{ref} value, then the difference will be subtracted from the reference voltage amplitude.

Otherwise, it will follow the traditional Q/E droop equation. Many contributions have been made to enhance the system operation using adaptive droop control. In [27], a second-order filter and a modified equation of voltage droop were used to enhance the reactive power sharing and transient response. In [28], the author implemented the adaptive integral loop technique, improved power-sharing dynamic response, and reduced the circulating current by removing the effect of the line impedance. In [29], the author calculated the microgrid line impedances and used it to calculate the adaptive droop parameters to ensures effective power-sharing and reduces line losses.

2.3.4.3. ***P/V droop control.*** In small size microgrid, the line impedance is considered more resistivity than inductive [30], which causes the change in the power equations used in P/f droop control. With the dominating resistive component, the effect of line reactance can be neglect. The main advantage of this method is that it has a more accurate representation of low voltage microgrid, which will lead to better active power-sharing and a more stable system [30]. The combination of $P-V$ and $Q-f$ was also encompassed in [31] to estimate and enhance the power-sharing capability of microgrids that operate autonomously. The $P-V$ and $P-f$ droop control inoculated in [30] improved power-sharing during export of power considering the line losses.

2.4. Feedback Controllers

In this section, the focus of the review will be the feedback controllers used mainly in the inner current loop of the Droop control structure. Several controllers are used for the inner current control loops, such as PI, synergetic, backstepping, state-feedback, and sliding Mode controllers.

2.4.1. PI control. PI control is the most popular controller due to its simplicity. The controller has two parts: proportional control part and integral control part. Proportional control is used to have a control transient response time, where the system reaches a steady state. The problem of proportional control is that it does not guarantee zero steady-state error, which leads to the usage of the integral controller, thus PI

controller. The control law $u(t)$ of PI control can be written as:

$$u(t) = K_p e(t) + K_i \int_0^t e(t)dt \tag{1}$$

The proportional gain K_p and the integral gain K_i are designed to achieve optimum performance for a single operating condition. Any change in the operating condition will result in reducing the performance of the controller.

PI controller is used in the inner and outer loops control in droop control structure. [32] used distributed PI control to reduce transient power loss in droop controlled base microgrid. Moreover, PI controllers are also used with different types of droop control like adaptive droop control [33] [34], VI Droop control [35] [36] and P/V droop control [37].

2.4.2. Synergetic control. In the literature, synergetic control was used to control the inner loop of droop control. The synergetic control is a nonlinear type of control developed by Russian scientist Kolesnikov [38] [39]. The basic concept of the control technique follows the design of Aggregated Regulators (ADAR). The objective of the control is to derive the system trajectories into a manifold defined by a macro-variable, where the macro-variable is determined based on the design specifications [40]. Assuming the macro-variables that defined the desired manifold expressed at:

$$\Psi = \psi(x, \dot{x}) \tag{2}$$

To find the control law for the synergetic control, it is required to solve the synergetic control evolution constraint function defined as:

$$T\dot{\Psi} + \Psi = 0, \;\; T > 0 \tag{3}$$

where T is a positive constant that defines the speed of convergence and *Psi* is the desired manifold.

The synergetic control theory and sliding mode control have a similar working concept, where force the closed-loop system to move on the desired manifold. However,

synergetic control is a chattering free technique the does not have a discrete control action as sliding mode control. On the other hand, the performance of synergetic control becomes less robust against model parameter uncertainties.

2.4.3. Backstepping control. Backstepping control is also used with droop control, where it is a strict feedback type of controller. The design procedure breaks the full system into a sequence of sub-systems and then steps backward recursively to apply the Lyapunov function stabilizing each outer sub-system in the entire system. The process terminates when the final external control is reached [41]. The control technique is a nonlinear controller designed by Serbian scientists Petar V. Kokotovic and others in the 1990s [42]. Backstepping ensures asymptotic stability [43] and design flexibility by evading the cancellations of useful nonlinearities [44]. Due to the general structure of the backstepping control algorithm, its control law could be complex to implement. The dynamic transient is slower, which is considered one of the drawbacks of backstepping control [43]. Considering the system [45]:

$$\dot{\eta} = f(\eta) + g(\eta)\xi \tag{4}$$

where to stabilize the system in Eq. 4, it is required to define a virtual stabilization input to the system to be as:

$$\dot{\eta} = [f(\eta) + g(\eta)\phi(\eta)] + g(\eta)[\xi - \phi(\eta)] \tag{5}$$

$$\dot{\xi} = u \tag{6}$$

then it the resulted system is:

$$\dot{\eta} = [f(\eta) + g(\eta)\phi(\eta)] + g(\eta)z \tag{7}$$

$$\dot{z} = u - \dot{\phi} \tag{8}$$

where to have a stable closed loop system, it is necessary to stabilize the two resulted subsystems in Eq. 7

2.4.4. State-feedback. State-feedback control is a controller that uses the state-space modeling of the system to follow the desired reference. The main advantage of this controller is that it is suited for multi-input multi-output systems. This makes state-feedback a very strong controller when it comes to secondary control in AC micro-grid. The working principle of state feedback depends on the state space representation, as a variable victor K is multiplied by the measured state variables x and subtracted from the reference signal r. The control law can be written as :

$$u = r - Kx \tag{9}$$

pole placement method is used to define the victor K. State-feedback control and a state observer were used for a combined voltage, and current loops in droop controlled islanded microgrid in [46] to achieve the required voltage and frequency. Furthermore, the method used shows good results on voltage harmonics mitigation.

State-feedback with disturbance rejection technique was used in [47] to output current, which tracks the reference accurately. The paper used partial input saturation to reduce the integral effect of the voltage and frequency regulation. Even though it is a robust controller, it has some weaknesses, such as the dependency on the module's accuracy, which means that the controller needs a lot of inputs to reach acceptable accuracy. This translates to a huge number of sensors needed for physical systems. Such weakness can be solved by implementing an observer to estimate the unreadable states.

2.4.5. Sliding mode control. Sliding Mode Control (SMC) is a well-known nonlinear robust controller with an assertive behavior against external disturbances and uncertainties. Due to its unique features, it does not require exact modeling to the system under study. It is enough to define a sliding surface and control low to take the system states from any state to the defined sliding surface and slide toward the equilibrium point. The concept of sliding mode was developed in the Soviet Union by Vadim Utkin originated from the concept of variable structure system [48] [45]. Despite its remarkable performance, it suffers from an undesired phenomenon known as the "Chattering", which is an uncontrolled switching frequency with finite amplitude [49].

Number of modifications were suggested by researchers to overcome th such as smooth time-varying compensator [50], power rate reaching mode [51], exponential sliding mode control [52] and high order sliding mode control [53].

2.5. Inverters

The raised demand on the distributed energy resources (DER) and their integration in the distribution systems directed the researchers' attention to the interface circuits between these DERs and the distribution systems. Inverters play a vital role in interfacing between these DERs and the power system.

Conventional inverters suffer from high total harmonic distortion (THD), switching losses, switch voltage and current stresses, and high voltage levels as well [54]. These problems required improvement in the conventional inverter structure, which leads to the implantation of multilevel inverters topologies. The multilevel inverters proved their ability to improve all the problems faced by conventional inverters. Nowadays, multilevel inverters play a main role in the distribution systems [55].

Multilevel inverters can be categorized under three main types: Cascaded H-bridge inverter, flying capacitor inverter, and diode-clamped multilevel inverter [56]. A diode-clamped inverter is proven to be a competitor in performance compared to the cascaded H-bridge, and superior to the flying capacitor inverter for the same number of levels [57]. The edge that the diode clamped inverter has over the cascaded H-bridge is the simpler control mechanism shown in [56]. Another main advantage for the diode-clamped inverter over other types is the shift of the total harmonic distortion centered on twice the switching frequency [57].

One of the focal points in this thesis is designing and implementing an improved analog switching modulation and drive circuits for the three-phase five-level diode-clamped inverter. This part of the literature survey reveals few publications tackle experimentally the switching modulation/drive circuits of the multilevel inverter. Several methods of switching modulations for the multilevel inverters are presented in [58] [59] [60].

These publications shed light on effective multi-carrier switching modulation techniques called phase-disposition pulse width modulation (PD-PWM), phase oppo-

sition disposition pulse width modulation (POD-PWM), Alternative phase opposition disposition pulse width modulation (APOD-PWM), and Phase Shift pulse width modulation (PS-PWM) for different types of multilevel inverters. Both PD-PWM and POD-PWM are used to control multilevel inverters, and reduced switch multilevel inverters [61]. In [62], the phase shift multi-carrier is used for the cascaded multilevel inverter. It is proved in this paper that this switching modulation can reduce the ripple and high-frequency harmonics of generated voltage.

A comparative study is conducted on the different multi-carrier switching modulations on the switched capacitor multilevel inverter in terms of the THD and voltage stresses on power switches [63]. The outcome of this comparative analysis is deduced using simulation results. More emphasis is given to the switching modulation (PD-PWM) for the single-phase diode-clamped inverter [64] and for three-phase diode-clamped inverter [65] [66]. PD-PWM is considered a very effective switching modulation for the diode-clamped inverters in power system applications.

The diode-clamped multilevel inverter is used in many fields, such as dynamic voltage restorer that stabilizes the voltage in the distribution system [67] and as DSTATCOM to stabilize the voltage [68] [69]. Diode clamped multilevel inverter is also used for the wind-based renewable energy systems [70].

Table 2.1: Summary of feedback control techniques used in droop control.

Technique	advantages	disadvantages
PI control	Simple control structures	Sensitive to the operating conditions
Synergetic control	Provides chattering free control action with global stability to the system under control	Less robust with respect to model parameter uncertainties
Backstepping control	Design flexibility	System dynamics and the external disturbance should be known
State-feedback	Simple and powerful for multi input/output systems	Requires a very accurate mathematical representation of the system under study
Sliding Mode Control	Provides robust and reliable performance with respect to model parameters uncertainties	The chattering phenomenon

Table 2.2: Summary of power control in microgrid.

Power control techniques	advantages	disadvantages
Centralized control	• Accurate equal current sharing between DGs in the same microgrid.	• Single point of failure. • Require high bandwidth communication channel between DGs and POI.
Master-slave control	• Good power management. • High voltage and frequency stability at POI.	• Slave control units cannot independently. • Cannot react to the variations happened by the load power. • need bandwidth communication link between master unit and slave units.
Distributed current control	• Good transient response. • minimizes the circulating currents between DGs.	• only used with balanced power systems. • Need for low bandwidth communication link between DGs.
Droop control	• Does not need any communication between DGs. • High adaptability to sudden changes in microgrid.	• Poor dynamic performance. • Poor harmonics sharing. • Power sharing is affected by inequality of line impedance of each inverter. • Poor voltage regulation.

2.6. Conclusion

The literature review of this thesis discussed the microgrid structure and modes of operation. The focus of this review was the power sharing techniques in islanded microgrid. The selected power sharing control method is droop control which requires two feedback control loops. Several feedback controllers used in droop control were discussed. Moreover, Dc to AC inverter typologies and operation were addressed.

Chapter 3: Control Scheme

3.1. Scheme

The focus of this chapter is to discuss the structure of the microgrid as well as the design of the droop control as well as state feedback and sliding mode control as the feedback controllers required to operate droop control based microgrid.

3.2. Droop Control

The droop controller operation starts with calculating the injected active and reactive powers using the transmission line impedance. By assuming that the transmission line impedance to be mainly inductive reactance (X) as shown in Figure 3.1, the output active power (w) and reactive power (var) of each DG is shown as:

$$P = \frac{EVsin(\alpha)}{X} \tag{10}$$

$$Q = \frac{EVcos(\alpha) - V^2}{X} \tag{11}$$

For a small value of the power angle α, so that sin(α) = α and cos(α) = 1, the active power P is directly proportional with α and reactive power Q is directly proportional with the deference between the voltage ant the inverter output E (V) and the voltage at the point of interconnection V. One method to change the power angle α it to vary the angular frequency of the inverter generated voltage ω (rad/s). For this case, the relation between P and ω and the relation between Q and E in any DG are shown respectively, as follows:

$$\omega = \omega^* - \frac{\Delta\omega}{P_{max}}(P - P_{ref}) \tag{12}$$

$$E = E^* - \frac{\Delta E}{Q_{max}}(Q - Q_{ref}) \tag{13}$$

where $\omega^*, E^*, P_{ref}, Q_{ref}, P_{max}$ and Q_{max} are the rated frequency, rated voltage, reference active power, reference reactive power rated active power and rated reactive power. The coefficients of the active power difference and reactive power difference are called

droop coefficients, and by using m and n as symbols for the coefficients the equations can be written as follows:

$$\omega = \omega^* - m(P - P_{ref}) \tag{14}$$

$$E = E^* - n(Q - Q_{ref}) \tag{15}$$

The reference signals generated from E and ω are compared with the output voltage. The error is used as an input of a feedback controller to generate a reference current. Then the reference current is compared with the output current. The current error is used to generate the reference signals for the inverter. Droop control structure is shown in Figure 3.2.

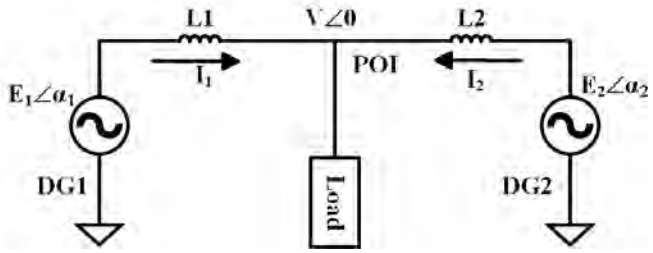

Figure 3.1: Simplified structure of the microgrid.

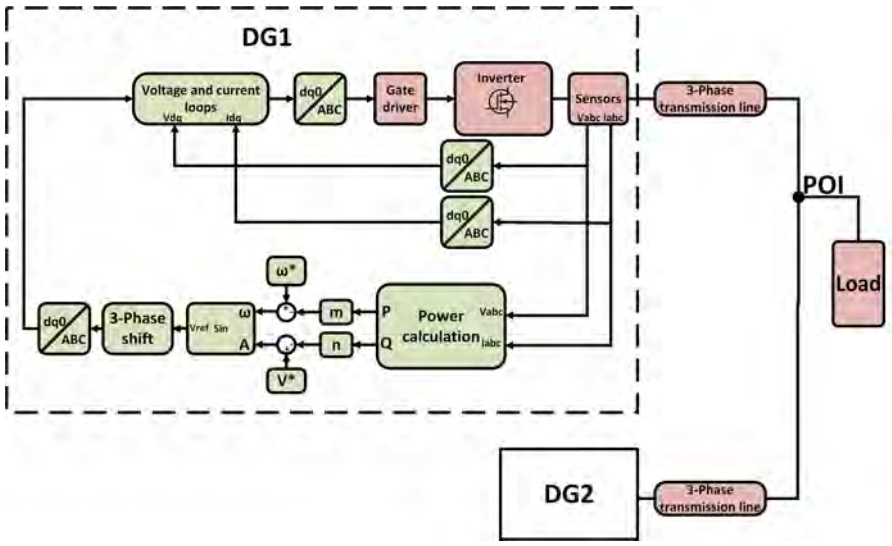

Figure 3.2: Conventional 3-phase droop control structure.

To further improve the performance of droop control in reactive power sharing virtual impedance is added the voltage and current loops. One of the objectives of the virtual impedance droop control is to enhance the reactive power sharing between the DGs since it is affected by the imbalance of the line impedances connected to DGs. This control modifies the reference voltage before entering the voltage and current loops making the equation of the reference:

$$V_{ref} = V_{ref-old} + Z_v I_{output} \tag{16}$$

where Z_v is the virtual impedance, Figure 3.3 shows the block diagram for virtual impedance loop-based droop control.

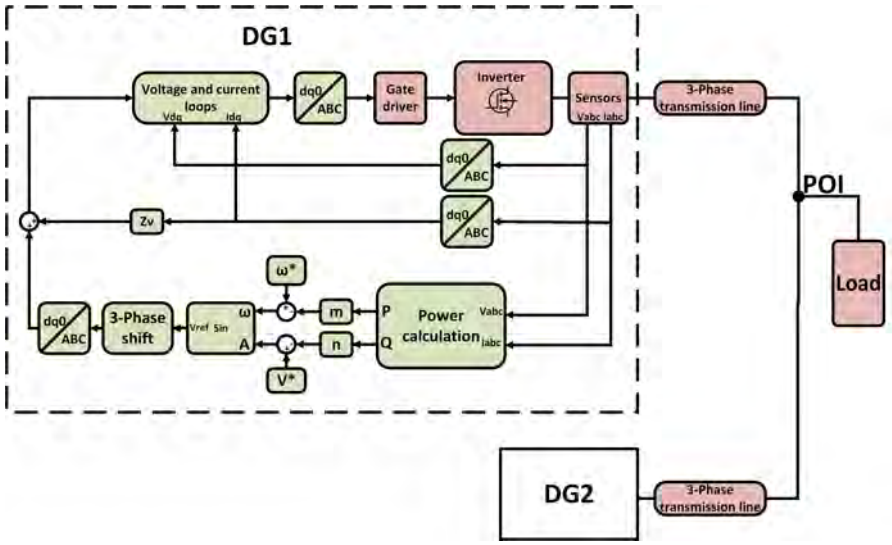

Figure 3.3: Virtual impedance 3-phase droop control structure.

3.3. Proposed Feedback Controllers

In this thesis, several control schemes have been used for the inner current loop, PI control, sliding mode control (SMC), exponential sliding mode control, and state feedback control. The PI controller is considered to be the conventional control method in the droop system, and it does not require a lot of knowledge of the system, while the other controllers need some parameters of the system in the form of a state-space model.

3.3.1. Model of the system for SMC. Figure. 3.4 demonstrates a simplified structure of the microgrid under study. The system consists of two inverters based DGs equipped with LC filters. The inverter used in this work is a 5-level diode clamped half-bridge inverter. Both inverters are connected to the point on interconnection (POI) by a transmission line, represented by a series RL impedance to supply the load with the required active and reactive power equally. To find the needed mathematical model, the output current I_{DG} in (A) must be found using V_{DG} and (V_L). The equation of I_{DG} using ohms-law is presented below,

$$
\begin{aligned}
I_{DG} &= \frac{V_{DG} - V_L}{R_1 + sL_1} \\
(R_1 + sL_1) I_{DG} &= V_{DG} - V_L \\
L_1 \dot{I}_{DG} &= V_{DG} - V_L - R_1 I_{DG} \\
\dot{I}_{DG} &= \frac{1}{L_1} V_{DG} - \frac{1}{L_1} V_L - \frac{R_1}{L_1} I_{DG}
\end{aligned} \tag{17}
$$

to control this 3-phase system, Eq. (17) must be presented in the following equations

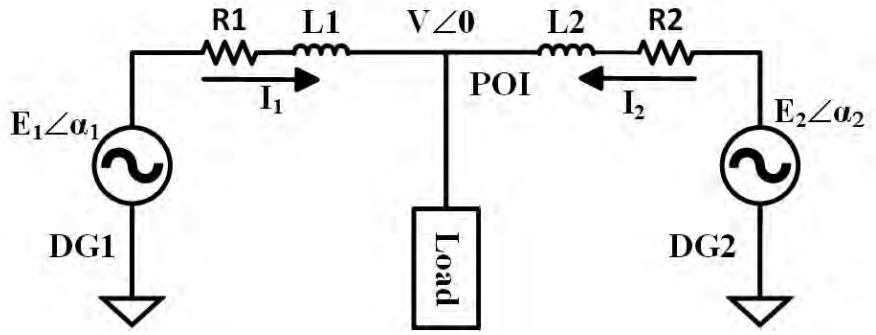

Figure 3.4: Simplified structure of the micro-grid under study.

in (dq) synchronous frame:

$$
\dot{I}_{d-DG} = -\frac{R}{L} I_{d-DG} + w I_{q-DG} + \frac{1}{L}(V_{d-DG} - V_{d-L}) \tag{18}
$$

$$
\dot{I}_{q-DG} = -\frac{R}{L} I_{q-DG} - w I_{d-DG} + \frac{1}{L}(V_{q-DG} - V_{q-L}) \tag{19}
$$

where I_{d-DG} , I_{q-DG} ,V_{d-DG} , and V_{q-DG} are the DG output currents and voltages in the (dq) frame; V_{d-L} , and V_{q-L} are the voltages at the POI in the (dq) frame; R_1 and L_1 are the equivalent series resistance and inductance of the feeder that is connecting the DGS with POI; Eq. (18) and Eq. (19) are considering the direction of the current from the DG to POI.

$$\begin{bmatrix} \dot{I}_{d-DG} \\ \dot{I}_{q-DG} \end{bmatrix} = \begin{bmatrix} -\frac{R}{L} & w \\ -w & -\frac{R}{L} \end{bmatrix} \begin{bmatrix} I_{d-DG} \\ I_{q-DG} \end{bmatrix} + \begin{bmatrix} \frac{1}{L} & 0 \\ 0 & \frac{1}{L} \end{bmatrix} \begin{bmatrix} V_{d-DG} \\ V_{q-DG} \end{bmatrix} + \begin{bmatrix} -\frac{1}{L} & 0 \\ 0 & -\frac{1}{L} \end{bmatrix} \begin{bmatrix} V_{d-L} \end{bmatrix} \tag{20}$$

$$y = \begin{bmatrix} 1 & 0 \\ 0 & 1 \end{bmatrix} \begin{bmatrix} I_{d-DG} \\ I_{q-DG} \end{bmatrix} \tag{21}$$

The state space Eq. (20) and Eq. (21) can be written as a first order system as:

$$\begin{aligned} \dot{x} &= Ax + Bu + Fd \\ y &= Cx + Du \end{aligned} \tag{22}$$

$$A = \begin{bmatrix} -\frac{R}{L} & w \\ -w & -\frac{R}{L} \end{bmatrix}, x = \begin{bmatrix} I_{d-DG} \\ I_{q-DG} \end{bmatrix}, B = \begin{bmatrix} \frac{1}{L} & 0 \\ 0 & \frac{1}{L} \end{bmatrix}$$
$$u = \begin{bmatrix} V_{d-DG} \\ V_{q-DG} \end{bmatrix}, F = \begin{bmatrix} -\frac{1}{L} & 0 \\ 0 & -\frac{1}{L} \end{bmatrix}, d = \begin{bmatrix} V_{d-sys} \end{bmatrix},$$
$$C = \begin{bmatrix} 1 & 0 \\ 0 & 1 \end{bmatrix}$$

3.3.2. Conventional SMC. The first step to build SMC is by defining manifold or sliding surface S where the sliding motion will occur [71], S can be expressed as:

$$S = e + \int \lambda e \tag{23}$$

where λ is a constant value that defines the speed of convergence to the sliding surface, and e is the error defined as:

$$e = x_{ref} - x \tag{24}$$

where x_{ref} is the reference variables victor and x is the feedback for the variables.

The next step is to design a control law that direct the system state trajectories to the sliding surface and to slide the trajectories toward the equilibrium point:

$$u = u_{dis} + u_{eq} \tag{25}$$

where u_{dis} is the discrete control that drives the system states to the sliding surface in the reaching mode, and u_{eq} is the equivalent control that guide the states on the sliding surface to the equilibrium point asymptotically [71] [51],

The Lyapunov's function (V) of stability is applied to assure the stability of the control system. Where it is required for the derivate of V to negative definite or semidefinite to achieve stability as [51]:

$$V = \frac{1}{2} S^T S \tag{26}$$

$$\dot{V} = \frac{1}{2}(S^T \dot{S} + \dot{S^T} S) = S^T \dot{S} \leq 0 \tag{27}$$

thus using Eq.(22) and Eq.(23) to find $\dot{S}$ leads to:

$$\begin{gathered}
\dot{S} = \dot{e} + \lambda e \\
\dot{S} = \dot{x}_{ref} - \dot{x} + \lambda (x_{ref} - x) \\
\dot{S} = \dot{x}_{ref} - \dot{x} + \lambda x_{ref} - \lambda x \\
\dot{S} = \dot{x}_{ref} + \lambda x_{ref} - \dot{x} - \lambda x \\
\dot{S} = \dot{x}_{ref} + \lambda x_{ref} - (Ax + Bu + Fd) - \lambda x \\
\dot{S} = \dot{x}_{ref} + \lambda x_{ref} - Ax - Bu - Fd - \lambda x \\
\dot{S} = \dot{x}_{ref} + \lambda x_{ref} - (Ax + \lambda x) - Bu - Fd
\end{gathered} \tag{28}$$

to satisfy Eq. (27) the reaching mode u_{dis} needs to be as:

$$u_{dis} = k\,sign(S) \tag{29}$$

Consequently, u_{eq} which will direct the states of the system to the stable state can be obtained from Eq. (28) as:

$$\begin{aligned} \dot{S} &= \lambda \dot{x}_{ref} - \lambda (Ax + Bu + Fd) = 0 \\ u_{eq} &= B^{-1}[\dot{x}_{ref} + \lambda x_{ref} - (Ax + \lambda x) - Fd] \end{aligned} \tag{30}$$

3.4. Proposed Control Schemes

As mentioned earlier, there are two contributions in control in thesis. One is to provide a control scheme consists of modifications to the conventional SMC control law and apply it on droop control microgrid, the other is to apply state feedback control on the same microgrid.

3.4.1. Hyperbolic tangent reaching Mode. The signum switching function (*sign*) in the conventional SMC leads to a high amount of chattering in the reaching mode due to its discontinuous behavior. To improve the performance of SMC, the signum function can be replaced by the hyperbolic tangent function ($tanh$). Where ($tanh$) provides smooth continuous behavior in the reaching mode [50]. Correspondingly, the discrete control law in Eq. (29) can be re-written as:

$$u_{dis} = k(S)\,tanh(\alpha S) \tag{31}$$

where, $\alpha < 1$ defines the decaying rate of the reaching mode as shown in Figure 3.5.

3.4.2. Exponential SMC. The conventional reaching law in Eq. (29) has a fixed control gain k, no matter if the system state trajectories are close or far away from the sliding surface ($S = 0$). Thus, the constant gain implements excessive gain control in the reaching mode for some cases. To avoid that, an Adaptive SMC technique is proposed that provides the required gain in the reaching mode based on the distance

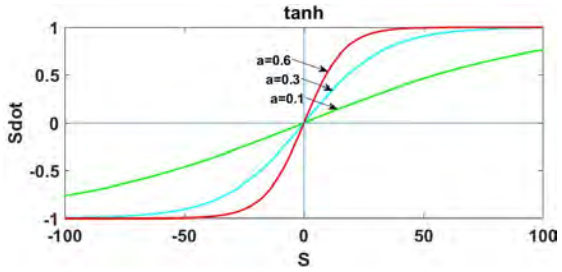

Figure 3.5: The Hyperbolic Tangent function *tanh*.

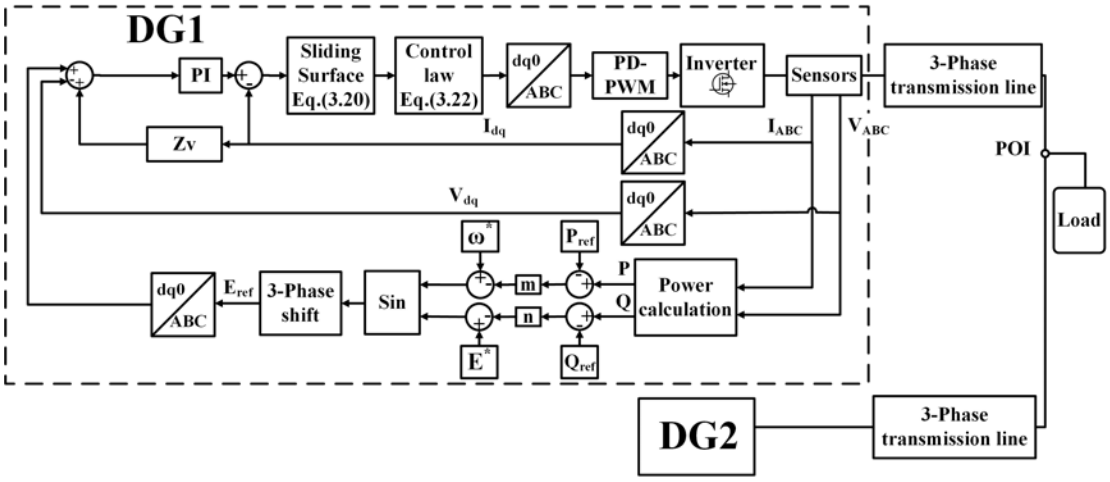

Figure 3.6: Block diagram of the droop control with SMC as inner current loop.

from the sliding surface. That is done by making the reaching mode gain k a function of S as:

$$u_{dis} = k(S)\, sign(S) \tag{32}$$

An exponential adaptive reaching mode is proposed in [52], which adapt to the variations of the value of (S) exponentially. As a result, exponential SMC successfully achieved better control on both the chattering and tracking performances, which is unattainable to be realized with the conventional sliding-mode control approach. Exponential SMC defined as:

$$u_{dis} = \frac{k}{N(S)}\, sign(S) \tag{33}$$

$$N(S) = \delta_0 + (1-\delta_0)e^{-\varphi|S|^p} \tag{34}$$

$$k \approx \frac{\delta_0 |S(0)|}{t_r} \tag{35}$$

$$\varphi \gg (\frac{1-\delta_0}{\delta_0|S(0)|})^{\frac{1}{p}} \tag{36}$$

where t_{rd} is the desired reaching time. To have an exponential SMC, the below should be considered:

- $1 > \delta_0 > 0$
- $\varphi >> 0$
- $p > 1$

performing stability check leads to:

$$\dot{V} = S^T \frac{k}{N(S)} sign(S) \leq 0 \tag{37}$$

For Eq. (37) to be stable $k > 0$. Implementing the hyperbolic tangent function along with the exponential SMC makes the discrete control law defined as:

$$u_{dis} = \frac{k}{N(S)} tanh(\alpha S) \tag{38}$$

The complete structure of the proposed control is illustrated in Figure 3.6. The system starts with calculating the active and the reactive power from the measured inverter 3-phase voltage and current. Then the resultant power will be compared with reference active and reactive powers. The difference is multiplied by the droop coefficients to generate voltage and frequency reference to be subtracted from the rated volage and frequency as given in Eq. (14) to get the reference voltage signal which will be sifted to form 3-phase voltage signal. Afterwards the park transformation is used to get the reference in dq format, which will reduce the number of feedback loops from 6 loops to 4 loops. The two outer loops are the voltage control PI loops, and the 2 inner current loops are the proposed controller.

3.4.3. State feedback control. State feedback is a simple control yet a powerful control. The control method depends on the linear state space representation:

$$\begin{aligned} \dot{x} &= Ax + Bu \\ y &= Cx + Du \end{aligned} \tag{39}$$

where x is the state variables victor, u is the input of the system and y is the output. The controller uses all the state variables multiplied by control constants vector k, so that the output follows the reference input. The design of the controller is basically finding proper values for k vector. The system with the controller block diagram is shown in Figure 3.7.

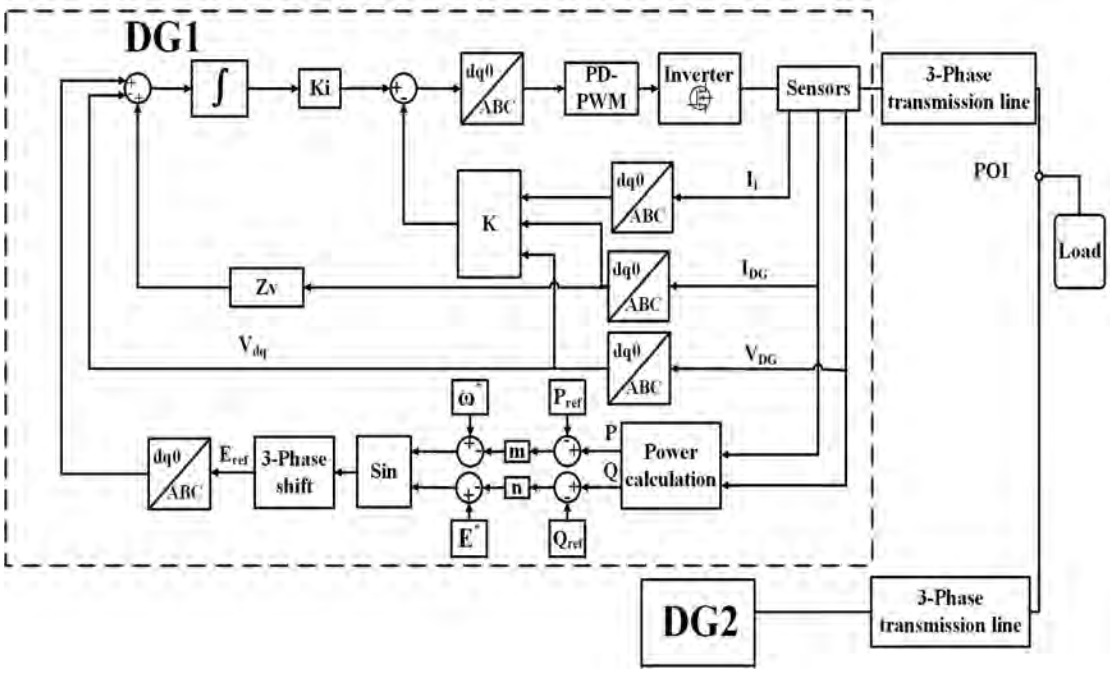

Figure 3.7: Structure of droop with state feedback control.

3.4.3.1. ***Model of the system for state feedback.*** The model of the system for state feedback requires a more detailed structure of the microgrid than the one used for the sliding mode control. The detailed structure must contain the filter parameters as in Figure 3.8.

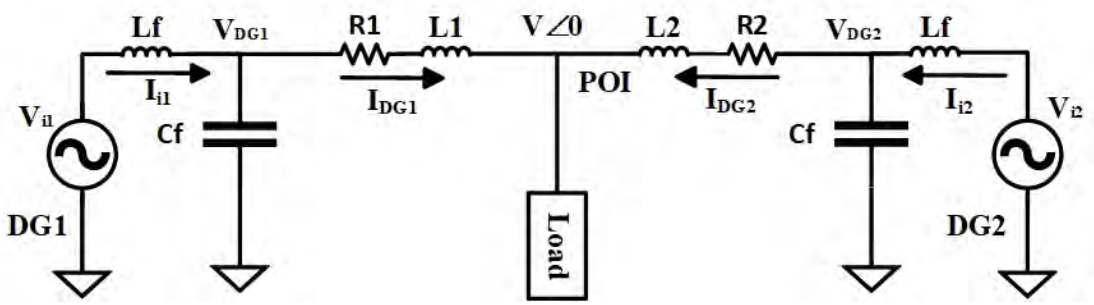

Figure 3.8: Microgrid structure for state feedback.

The state variables for used in model the system are the DG output current I_{DG},DG output voltage $V_{DG}$and inverter output current I_i, while the inverter voltage is the input of the system. Using these variables, the state space equations will be Eq.18 along with:

$$\begin{aligned} \dot{V_{DG}} &= \frac{1}{C_f} I_i - \frac{1}{C_f} I_{DG} \\ \dot{V}_{d-DG} &= \frac{1}{C_f} I_{d-i} - \frac{1}{C_f} I_{d-DG} + w V_{q-DG} \\ \dot{V}_{q-DG} &= \frac{1}{C_f} I_{q-i} - \frac{1}{C_f} I_{q-DG} - w V_{d-DG} \end{aligned} \tag{40}$$

$$\begin{aligned} \dot{I}_i &= \frac{V_i}{L_f} - \frac{V_{DG}}{L_f} \\ \dot{I}_{d-i} &= \frac{V_{d-i}}{L_f} - \frac{V_{d-DG}}{L_f} + w I_{q-i} \\ \dot{I}_{q-i} &= \frac{V_{q-i}}{L_f} - \frac{V_{q-DG}}{L_f} - w I_{d-i} \end{aligned} \tag{41}$$

Using these equations and ignoring the disturbance caused by the other DG in the microgrid, the state space model of the system can be presented as follow:

$$A = \begin{bmatrix} 0 & w & -\frac{1}{C_f} & 0 & \frac{1}{C_f} & 0 \\ -w & 0 & 0 & -\frac{1}{C_f} & 0 & \frac{1}{C_f} \\ 0 & 0 & -\frac{R}{L} & w & 0 & 0 \\ 0 & 0 & -w & -\frac{R}{L} & 0 & 0 \\ -\frac{1}{L_f} & 0 & 0 & 0 & 0 & w \\ 0 & -\frac{1}{L_f} & 0 & 0 & -w & 0 \end{bmatrix}, x = \begin{bmatrix} V_{d-DG} \\ V_{q-DG} \\ I_{d-DG} \\ I_{q-DG} \\ I_{d-i} \\ I_{q-i} \end{bmatrix}, B = \begin{bmatrix} 0 & 0 \\ 0 & 0 \\ 0 & 0 \\ 0 & 0 \\ \frac{1}{L} & 0 \\ 0 & \frac{1}{L} \end{bmatrix}$$

$$u = \begin{bmatrix} V_{d-i} \\ V_{q-i} \end{bmatrix}, C = \begin{bmatrix} 1 & 0 & 0 & 0 & 0 & 0 \\ 0 & 1 & 0 & 0 & 0 & 0 \end{bmatrix}, D = \begin{bmatrix} 0 \\ 0 \end{bmatrix}$$

3.4.3.2. ***State feedback gains.*** The steps of designing state-feedback controller starts with checking the stability of the system, which can be achieved by finding the

eigenvalues of the matrix A. Then the system must be controllable, to check the controllability of the system can be check if:

$$\begin{bmatrix} B & AB & A^2B & \ldots\ldots A^{n-1}B \end{bmatrix} \tag{42}$$

has a rank equal to n.

The next step is designing k matrix by using pole-placement method. To understand this method, the value of reference r must be zero and D matrix is assumed to be zero. This will make the representation of the closed loop system as follows:

$$\begin{aligned} \dot{x} &= (A - BK)x + Bu \\ y &= Cx \end{aligned} \tag{43}$$

since,

$$u = r - Kx \tag{44}$$

where r is the reference signal.

The last step is to find the desired 2 most dominant poles and use them to solve for K matrix. The desired poles can be found using the desired settling time and overshoot of the controller to find the damping ratio ζ and the natural frequency of the system ω_n by using the following equations.

$$t_s = \frac{4}{\zeta \omega_n} \tag{45}$$

$$M_p = e^{-\frac{\zeta \pi}{\sqrt{1-\zeta^2}}} \times 100\% \tag{46}$$

where t_s is the settling time, M_p is the overshoot percentage. The damping ratio ζ and the natural frequency of the system ω_n relation to the poles s is presented in the following equation,

$$s = -\zeta \omega_n \pm \omega_n \sqrt{1 - \zeta^2} \tag{47}$$

the other poles are chosen to be multiples of the real part of the two dominant poles. To remove the effect of the disturbance integral gain must be multiplied with the error between the reference signal and the output. The gains can be found by adding two more poles to the system and solve for new K matrix. The last two columns in K matrix are used for the integral gain.

3.5. Conclusion

This chapter discussed the theory behind droop control and its derivation. Moreover, the mathematical model of the system understudy needed for the proposed control schemes has been derived. The chapter also showed the design of state feedback controller and hyperbolic tangent exponential sliding mode control scheme.

Chapter 4: Simulation Results

4.1. Introduction

This chapter shows the simulation results of virtual impedance droop control with different feedback controllers applied in voltage and current loops.

4.2. Droop Control Simulation Results

The simulation results are carried out using MATLAB/Simulink software. The performance of the proposed control schemes (hyperbolic tangent exponential SMC and state feedback control) are compared with conventional PI control and another two versions of SMC: conventional adaptive SMC and power rate SMC to prove the efficiency of both control methods.

In the simulations, the connected load impedance to the micro-grid, which is supplied with the required power by the parallel DG units (multi-level inverters), was changed from $180+55\,j\Omega$ to $90+27.5\,j\Omega$ at $t=4s$ and changed back to $180+55\,j\Omega$ at $t=7s$.

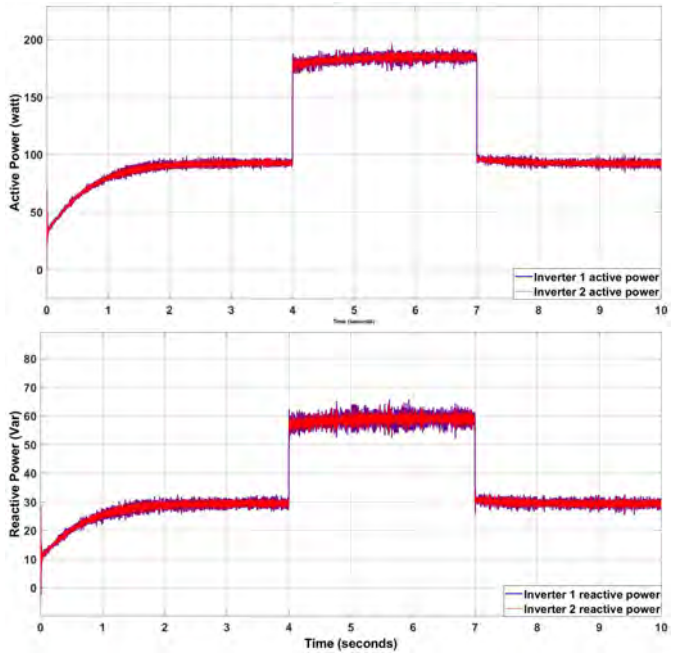

Figure 4.1: Active and reactive power sharing for droop control with conventional PI control.

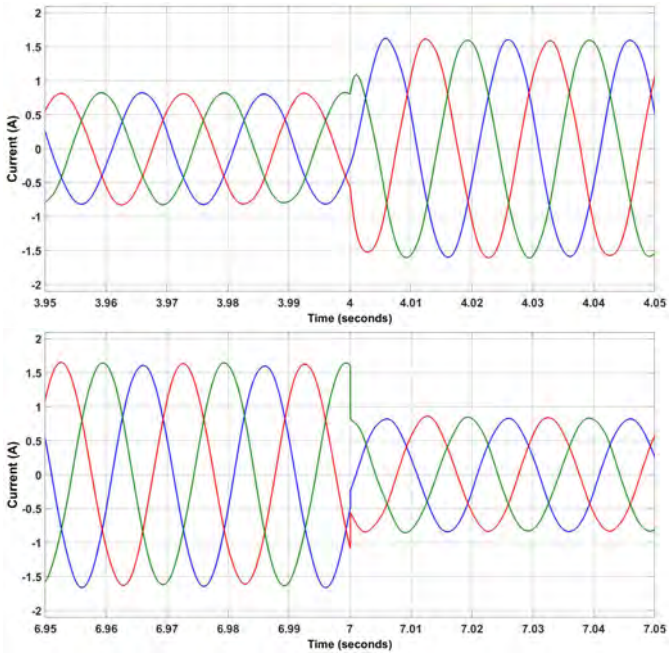

Figure 4.2: The three-phase current at POI during the sudden load change when using conventional PI control.

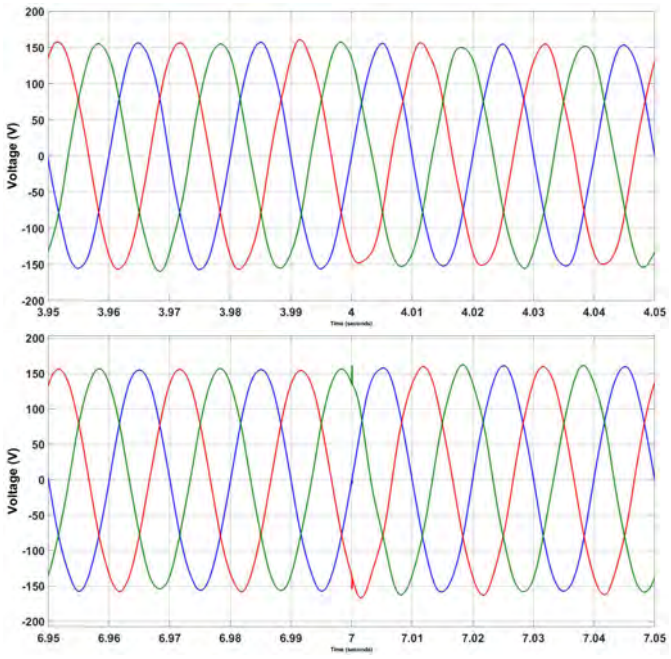

Figure 4.3: The three-phase voltage at POI during the sudden load change when using conventional PI control.

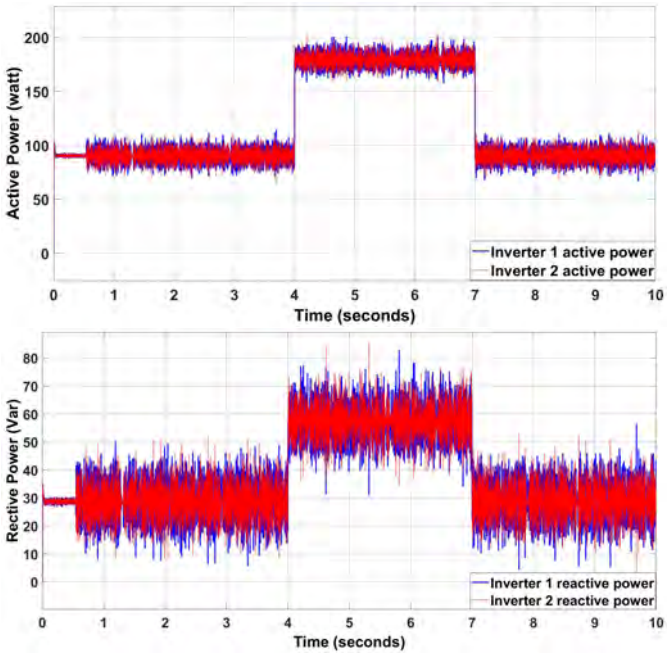

Figure 4.4: Active and reactive power sharing for droop control with adaptive sliding mode control.

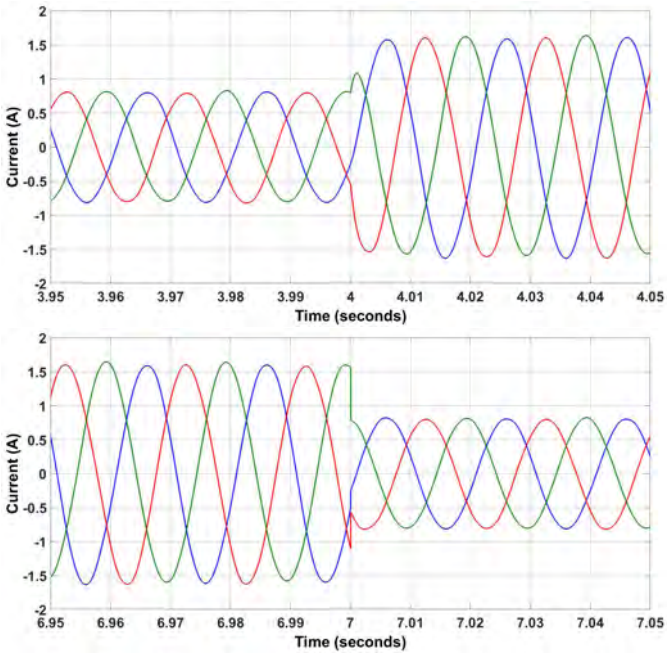

Figure 4.5: The three-phase current at POI during the sudden load change when using adaptive SMC.

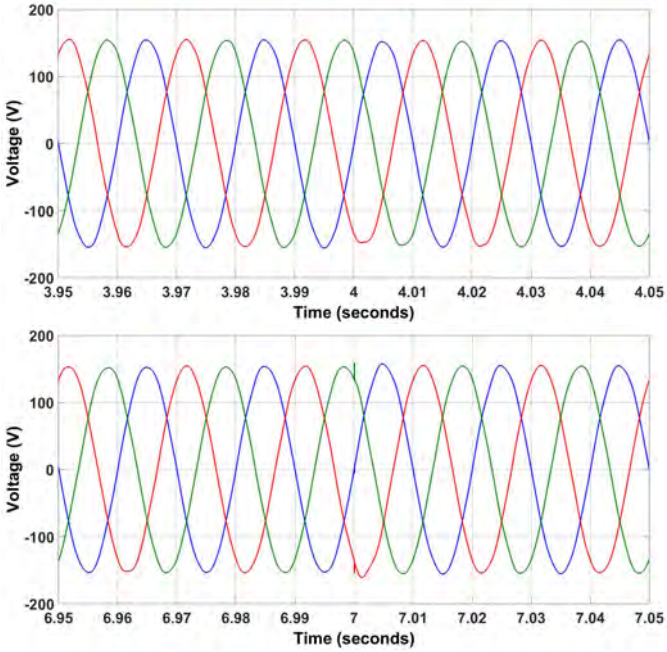

Figure 4.6: The three-phase voltage at POI during the sudden load change when using adaptive SMC.

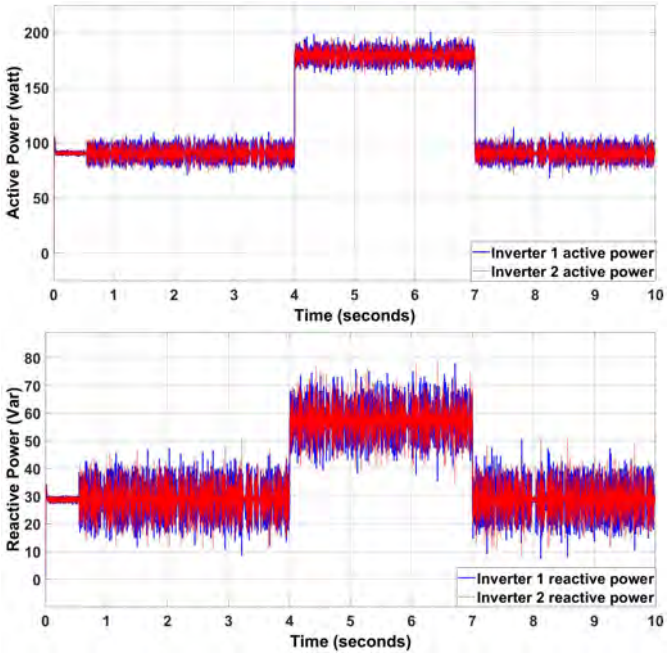

Figure 4.7: Active and reactive power sharing for power rate SMC with a sudden load change.

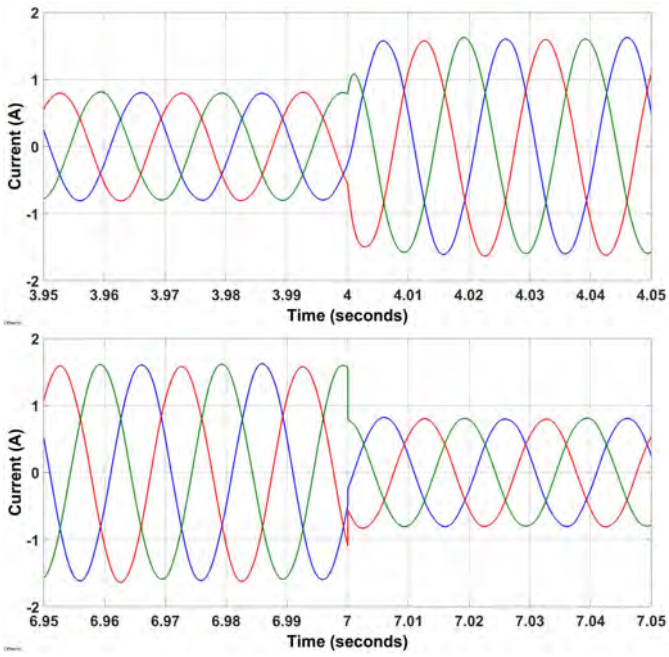

Figure 4.8: The three-phase current at POI during the sudden load change when using power rate SMC.

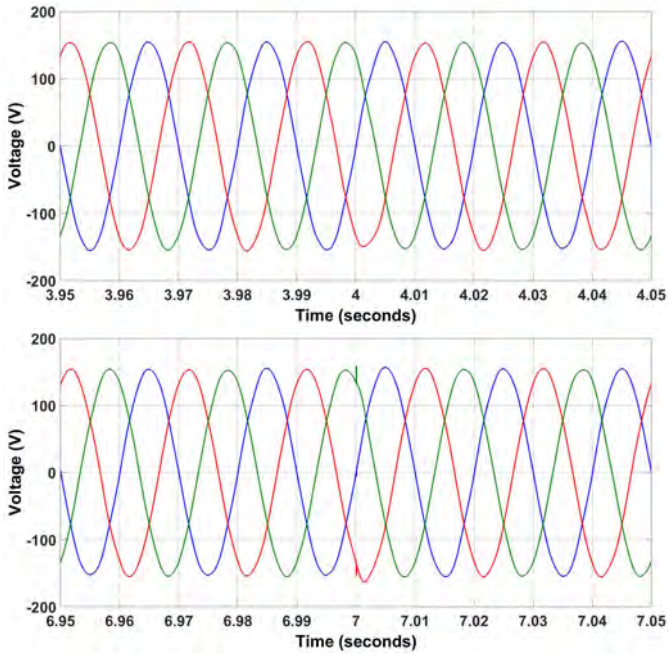

Figure 4.9: The three-phase voltage at POI during the sudden load change when using power rate SMC.

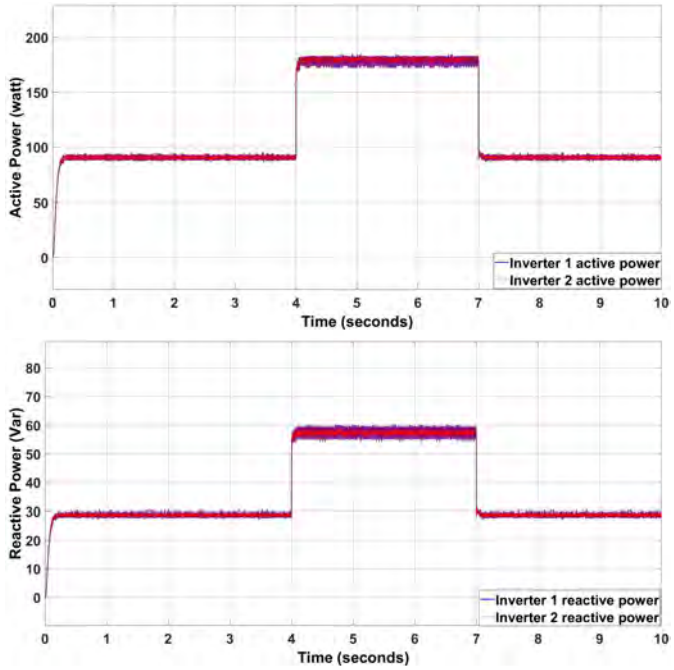

Figure 4.10: Active and reactive power sharing for exponential SMC with a sudden load change.

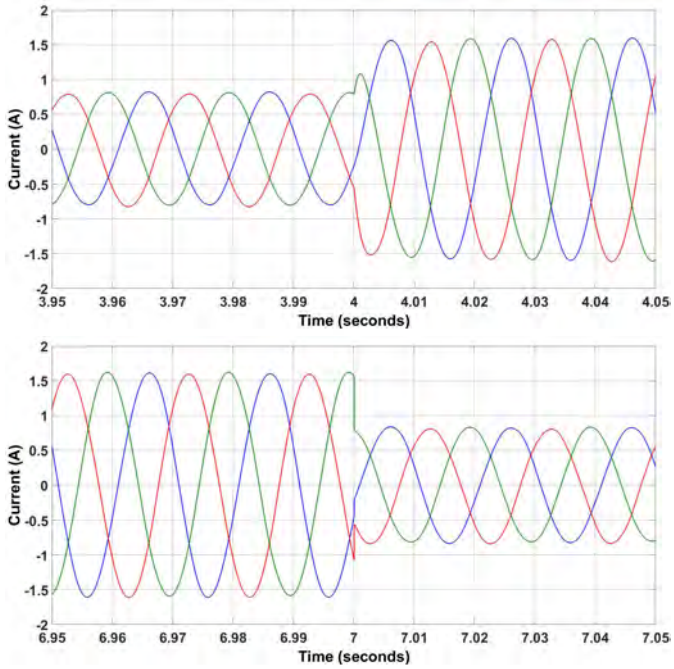

Figure 4.11: The three-phase current at POI during the sudden load change when using exponential SMC.

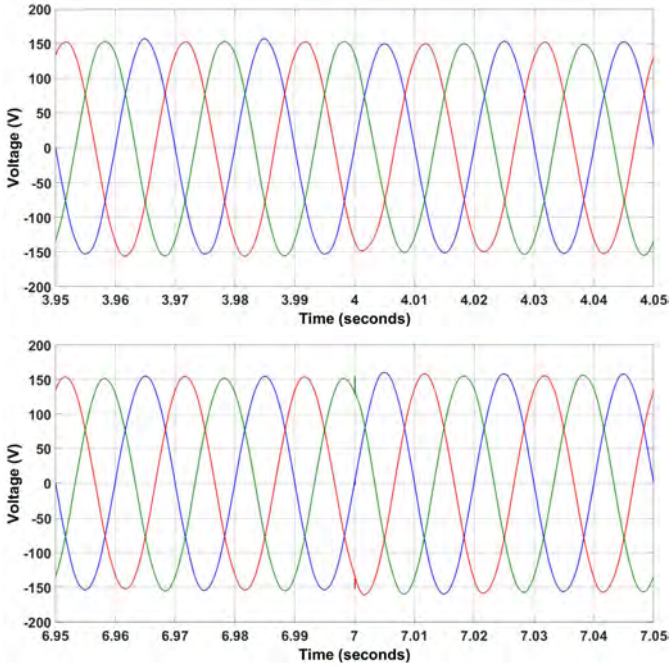

Figure 4.12: The three-phase voltage at POI during the sudden load change when using exponential SMC.

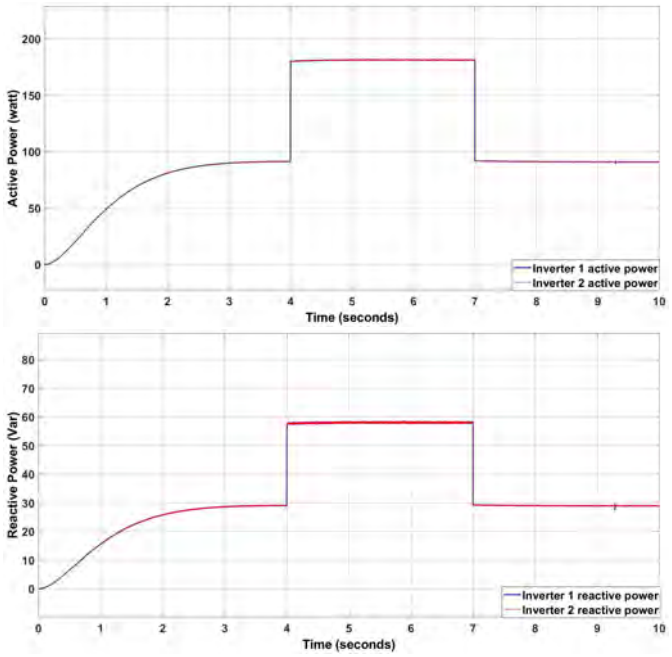

Figure 4.13: Active and reactive power sharing for droop control with state feedback control.

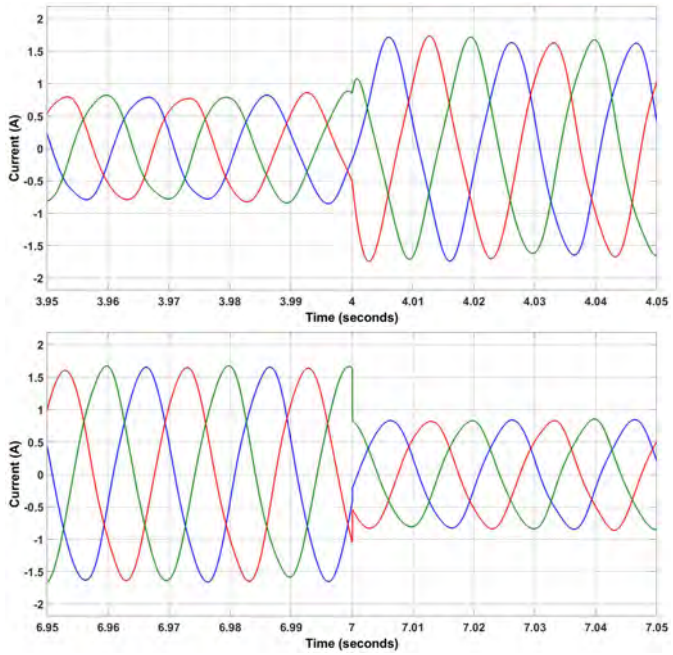

Figure 4.14: The three-phase current at POI during the sudden load change when using state feedback control.

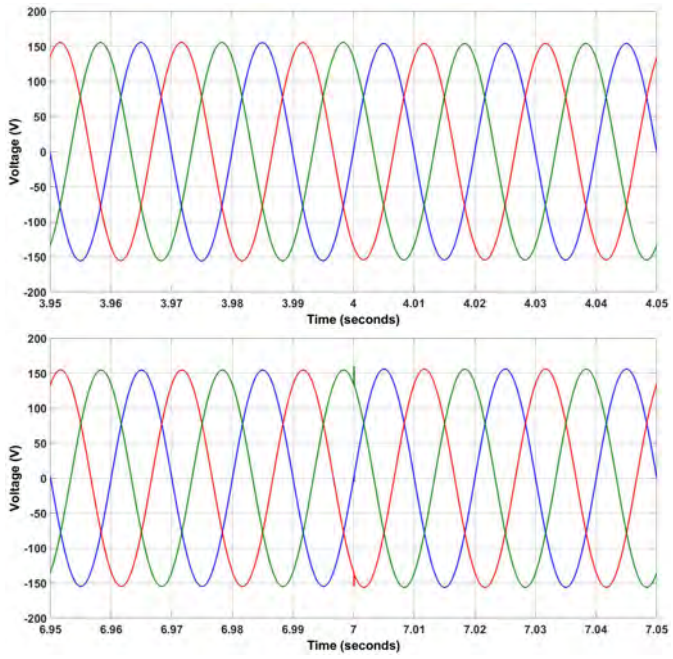

Figure 4.15: The three-phase voltage at POI during the sudden load change when using state feedback control.

The results for the active and the reactive power-sharing for the hyperbolic tangent exponential SMC and state feedback control in Figure 4.10 and Figure 4.13,respectively demonstrate the ability of those proposed schemes to allow DGs to accurately share the active and reactive power in microgrid compared to PI shown in Figure 4.1 control and other sliding mode control. Moreover, state feedback control shows better performance than the hyperbolic tangent exponential SMC in steady state and at sudden load change, while the latter shows a faster startup for the system. In addition, the hyperbolic tangent exponential SMC show a better ability to suppress the chattering in the injected active and reactive power compared to conventional adaptive SMC and power rate SMC that is shown in Figure 4.4 and Figure 4.7 respectively illustrate a weak performance against the chattering in the injected active and reactive power.

Figure 4.2 Figure 4.5, Figure 4.8,Figure 4.11 and Figure 4.14 shows the effect of the sudden load change on the current for each method. The same for the Figure 4.3 Figure 4.6, Figure 4.9 Figure 4.12 and Figure 4.15 that shows that effect on the voltage at POI.

4.3. Conclusion

The simulation results shows the effectiveness of the proposed control techniques in achieving accurate power sharing even with sudden load changes, as well as maintaining the voltage and current stability at POI.

Chapter 5: Experimental Setup

5.1. Introduction

This chapter discuss the structure of the experimental setup used in this thesis. It starts with a brief information about DSpace SCALEXIO Lab Box, the control unit, and its cards. Furthermore, the structure of the control and carrier generation circuits, followed by the drive circuit required to operate the power switches. Finally, the structure of the multilevel inverter for every DG.

5.2. DSpace SCALEXIO Lab Box

DSpace SCALEXIO Lab Box is a laboratory system that can be used as a real-time controller. It can address various applications that can range from automation, aerospace, medical, automotive, research, and more. Furthermore, DSpace SCALEXIO Lab Box is scalable to match a huge system with 18 I/O boards. Two processing units are used in DSpace SCALEXIO Lab Box, the SCALEXIO main processor unit, and the DS6001 Processor Board. The main processor is used for programs that require high computational performance, while the DS6001 Processor Board is suitable for fast closed-loop rates and high bandwidth of inputs and outputs.

Figure 5.1: DSpace SCALEXIO Lab Box

The boards used in this work are DS6101 Multi-I/O Board, DS6221 A/D Board, and DS6241 D/A Board. DS6101 Multi-I/O Board is a general-purpose board. It has up to 69 I/O ports that can operate signals with several voltage levels, 12V, 24V, and 48V, either as inputs or outputs. Moreover, the input-output I/O ports are divided to handle both analog and digital signals.

Figure 5.2: DS6101 Multi-I/O

DS6221 A/D Board serves as a high-speed input board for analog signals. In addition to 16 input ports with 16-bit resolution and as fast as 4MSample/s, all the input channels are differential, suited for non-common reference inputs. The voltage range of this board is +10V and – 10V.

Figure 5.3: DS6221 A/D Board

Finally, DS6241 D/A Board is an output board containing 20 channels with a separate 16-bit accuracy digital to analog converter for each channel. The output can cover the range of +-10V with an error of less than 1mV. Moreover, the sampling rate of each port can reach up to 500 KSample/s.

Figure 5.4: DS6241 D/A Board

The number of outputs (from DSpace to the system) used in this thesis is six analog signals with a range of +-1V and one digital signal with 10V output. Furthermore, the number of inputs (from the system to DSpace) is 18 analog signals with a range of =-5V inputs. Taking these requirements into consideration, the available boards are suitable for the required tasks.

5.3. Suggested Analog Circuits for Multicarrier PWM (PD-PWM)

This section shows the circuits that are used to generate the control signals and carrier signals. The parameters of all forthcoming circuits are given in Table 5.1.

5.3.1. Control signals. The control signals are needed for the switching modulation required for the operation of the multilevel inverter. To generate the required signals (control and carrier), some circuits are developed such as oscillators, PWM, and filtered square and triangular signals. The block diagram of all control circuits is illustrated in Figure 5.5. The regular oscillator chosen for this circuit needs the use of digital to analog converters (DAC) and filters. To avoid the complexity associated with the regular oscillator, another oscillator called Wien-bridge is selected with the amplitude stabilization, which is done by diodes. The proposed circuit of the utilized oscillator can be seen in Figure5.6. To choose the frequency of the oscillator, a considered formula for the positive feedback circuit is given as,

$$f = \frac{1}{2\pi RC} \tag{48}$$

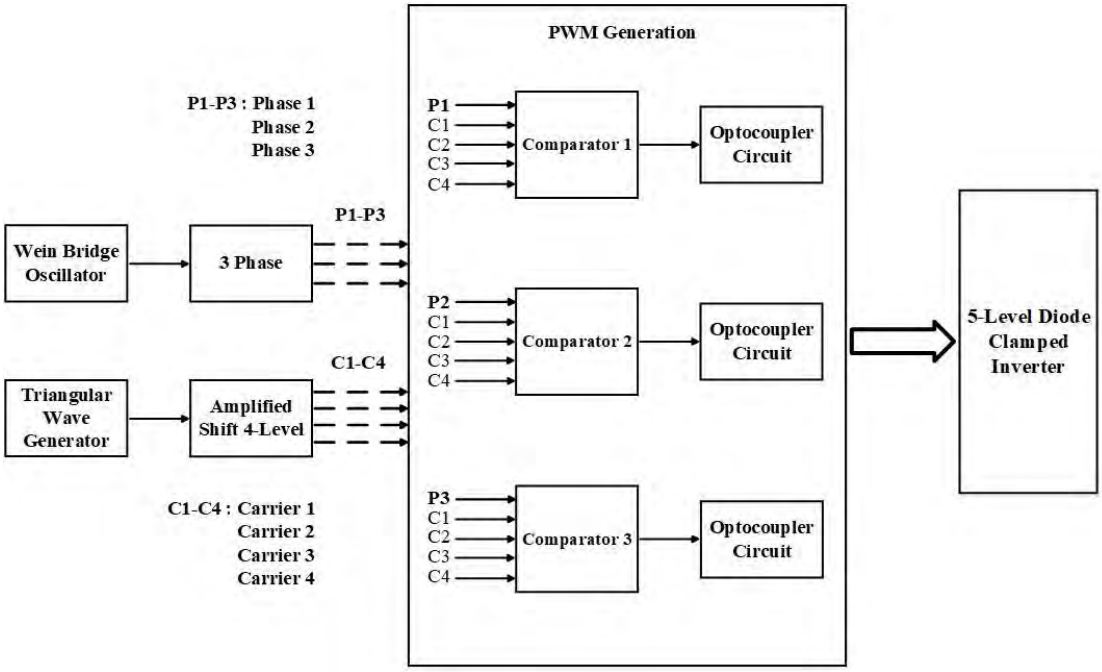

Figure 5.5: Block diagram of the diode clamped inverter control circuits.

where in Figure 5.6, $R5 = R6 = R$ and $C1 = C2 = C$. The values of the capacitors are selected so that the frequency is close to 50 Hz, while potentiometers were used as $R5$ and $R6$ to reach the required frequency (values given in Table 5.1). The values of the negative feedback resistors must be selected so that the gain is equal to 3 to have the required oscillation [72]. The amplitude of the signal can be controlled by placing a potentiometer at the output. The op-amp used for this circuit is TL081. The next stage is to create three-phase control signals with 120 degrees phase shift between phases, by combining op-amp circuits, inverting amplifier, non-inverting amplifier, and a weighted summer circuits, as shown in Figure 5.7. The PCB implementation for the circuit of Figure 5.7 is already given in Figure 5.6-b. The voltage of each phase is written as follows:

$$V_{ph1} = V_{in}\angle 0 \tag{49}$$

$$V_{ph3} = 2 * \frac{V_{in}\angle 180}{j\omega C_1 R_1} \tag{50}$$

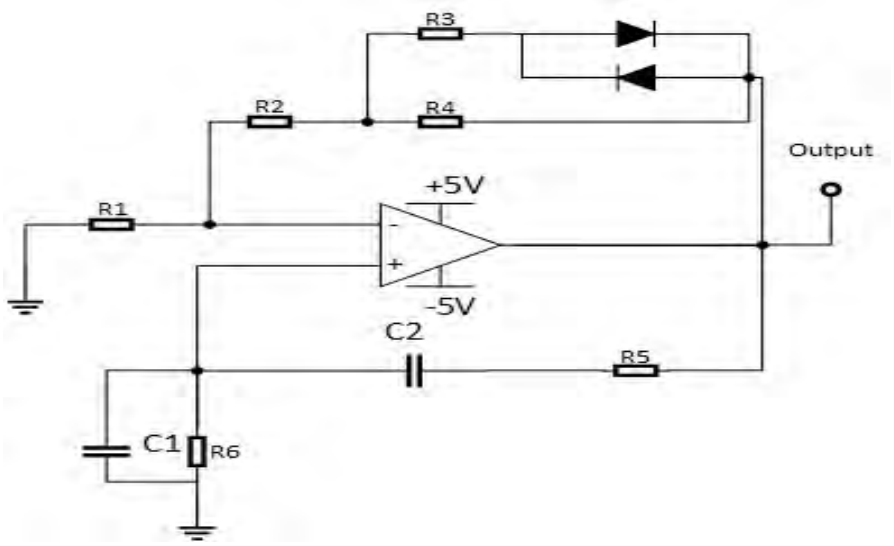

(a)

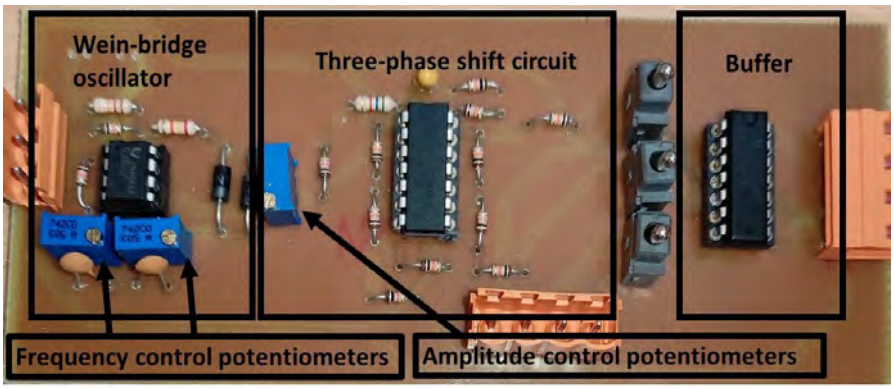

(b)

Figure 5.6: Circuit of control signal with amplitude stabilization, (a) circuit schematic, (b) its printed board.

$$V_{ph2} = -(V_{ph1} + V_{ph3}) \tag{51}$$

$R1$ and $C1$ are selected so that the phase of the voltage at the capacitor is equal to 240 degrees with respect to the input Vin.

5.3.2. Carrier signals. The control signals are compared with triangular (carrier) signals to generate the gating signals. The number of carrier signals must be equal to $(m-1)$ [55], where m is the number of desired levels. Since the inverter under study is the five-level diode-clamped inverter, then the four carrier signals with offset shifts are needed. Just like the sine control signal, the triangular signal can be generated by

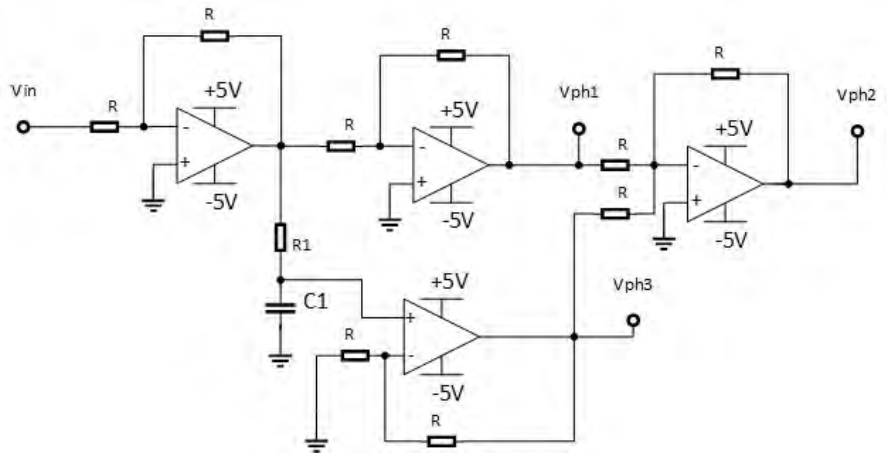

Figure 5.7: Three-phase shift circuit scheme for control signals.

many methods such as a simple square-wave generator circuit connected to an integrator circuit and a programmable device. Both methods can be used in this setup as shown in Figure 5.8.

The next stage is to vertically shift these carrier signals by certain values. By connecting the output of the triangular wave generator to four circuits of weighted adder, the four DC offset values are added to the carrier signals. The circuit schematics for the are shown in Figure 5.8 and Figure 5.9.

5.3.3. Design of suggested dead-band circuit for PD-PWM signals. To generate PWM output signals, the carrier and control signals must be compared to each other. The comparison can be done by a simple op-amp circuit. The output of the comparator should be used to generate the compliment PWM signal, which is needed for the compliment part of the inverter [55].

To prevent the short circuit caused by a switch and its compliment and to also reduce switching losses, a suggested dead-band (short-interval time between the signal and its compliment) is integrated within the PWM signals for each switch and its complement. Figure 5.10-a, Figure 5.10-b and Figure 5.10-c show the suggested dead-band circuit, drive circuit and its practical circuit, respectively. The dead-band formula for the circuit is designed based on the capacitor charging and discharging equations 52 and 53 respectively and the propagation delay difference of the NOT gates.

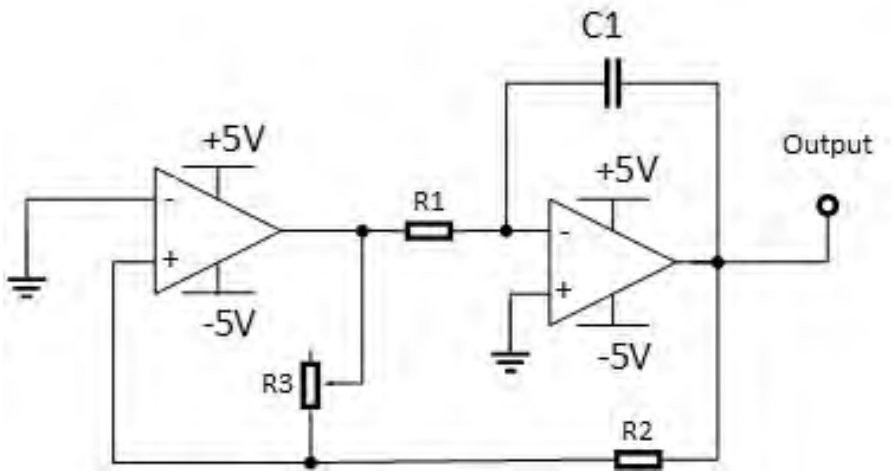

(a)

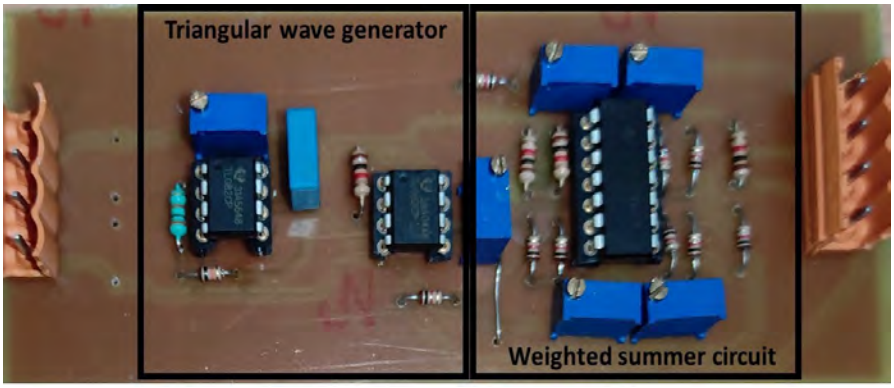

(b)

Figure 5.8: Triangular signal generator for carrier signals, (a) circuit schematic, (b) printed board.

$$V_C(t_c) = V_S(1 - e^{\frac{-t_c}{RC}}) \tag{52}$$

$$V_C(t_d) = V_S e^{\frac{-t_c}{RC}} \tag{53}$$

where V_C is the capacitor voltage in (V), V_S is the supply voltage in (V), t_c is the charging time in (s) of the capacitor and td is discharging time in (s). Form equations 52 and 53, the t_c and t_d in (s) equations can be written as,

$$t_c = RC * ln(\frac{V_s}{V_S - V_C}) \tag{54}$$

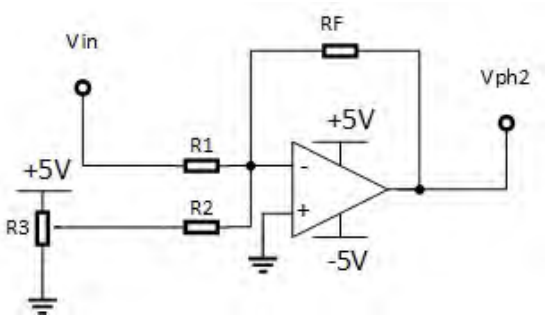

Figure 5.9: Weighted summer circuit scheme to make vertical shift for the carrier signals.

$$t_d = RC * ln(\frac{V_s}{V_C}) \tag{55}$$

The total dead-band time can be found by adding equations 54 and 55 and propagation delay difference of the NOT gates, which can be taken from the datasheet of the NOT gate directly.

$$T = t_c + t_d + t_p = RC * ln(\frac{V_S^2}{V_S V_C - V_C^2}) + t_p \tag{56}$$

where T is dead-band and t_p is the propagation delay in (s) difference of the NOT gates. The propagation delay for the used NOT gates (74AC04) is typically 4ns and the high-input voltage is 3.5V, and if the time for the dead-band is set longer than 10ns, (using R=47 Ω, VS =5V and V_C= High input voltage = 3.5V), then the value of the capacitor should be above 81.8pF. So, C=100pF is chosen since it is the next practical value; whereas, the theoretical dead-band time, (based on the exact capacitor value) is T =11.3ns.

5.4. Drive Circuit for Power Switches

The utilized power switch is the power MOSFET (FQA24N60). The power MOSFET needs a large current during its turning-on instant, and it is also required to discharge current from it during its turning-off instant [73]. Thus, the control circuits explained in the 2nd section are not qualified to supply/sink a large current during any

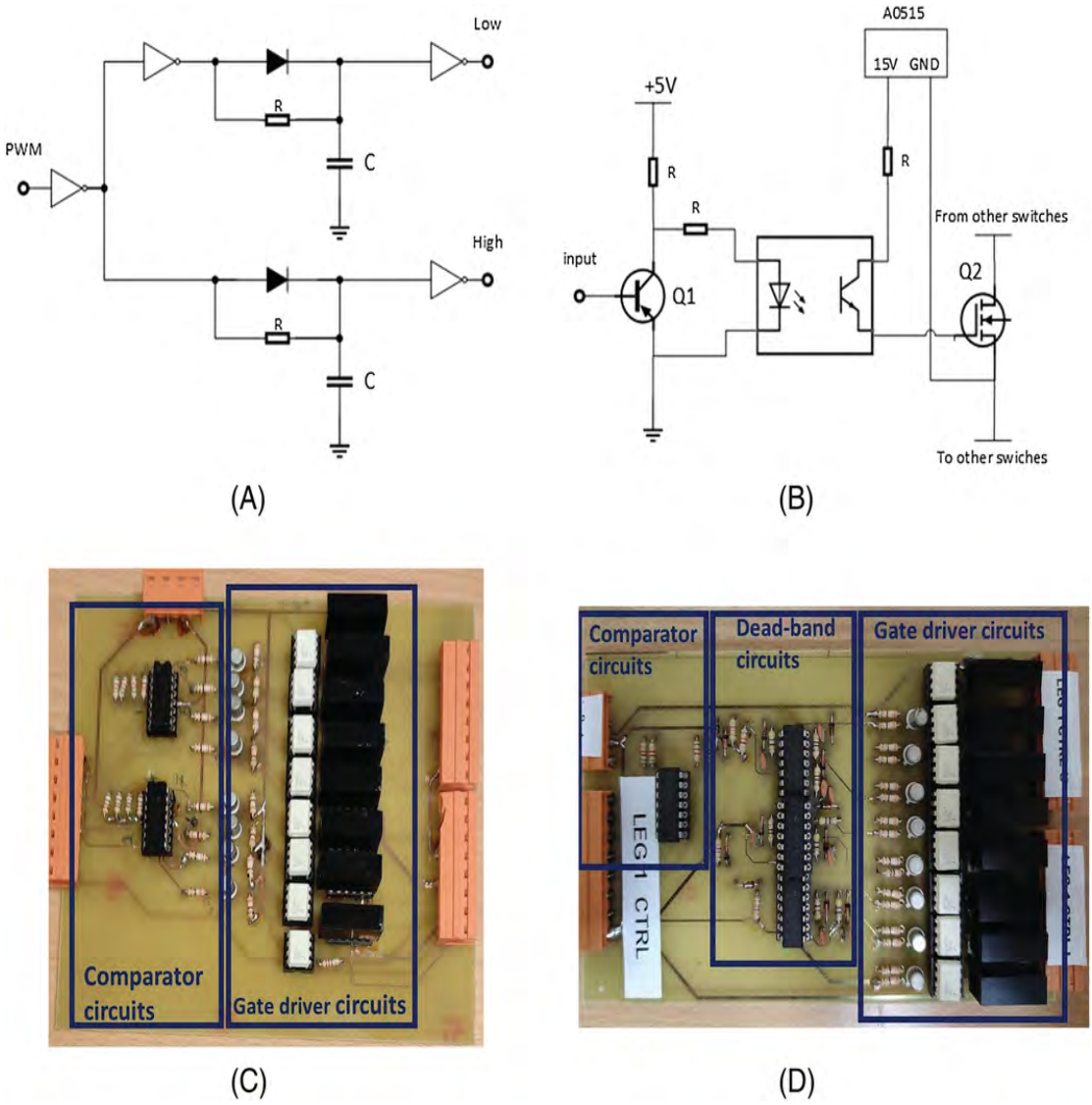

Figure 5.10: Dead-band and gate driver circuits and their printed circuits, (a) Schematic of the dead-band circuit, (b) schematic of drive circuit, (c) printed circuit without suggested dead-band circuit, (d) printed circuit with suggested dead-band circuit.

transition for the power MOSFET. A drive circuit is required to fasten this transition for power MOSFETs. The proposed drive circuit is depicted in Figure 5.10-b. The printed circuit of the conventional drive circuit (without dead-band) and the proposed drive circuit (with dead-band) are depicted in Figure 5.10-c and Figure 5.10-d, respectively.

The concept of the proposed circuit is that all PD-PWM signals are generated by the comparison of each phase control signal and four carrier signals, creating 8 PWM signals per phase. Each signal is fed to an opto-coupler circuit shown in Figure 5.10-b.

Table 5.1: Parameters of circuits in Fig.5.6 to Fig.5.10.

Parameters of circuit of Fig.5.6				
R1=R2	R3	R4	R5=R6	C1=C2
10kΩ	24kΩ	10kΩ	50kΩ	0.1μ F
Parameters of circuit of Fig.5.7				
R1		C	R	
5.6kΩ		1μ F	10kΩ	
Parameters of circuit of Fig.5.8				
R1		R2	C1	
10kΩ		30kΩ	0.1μ F	
Parameters of circuit of Fig.5.9				
R1		R2	Rf	
1kΩ		1kΩ	1kΩ	
Parameters of circuit of Fig.5.10.a				
R			C1=C2	
47Ω			100pF	
Parameters of circuit of Fig.5.10.b				
R			Q1	
220Ω			2n2222	

Each level of the inverter requires a separate isolated voltage source to prevent short circuit for the source of each the MOSFET. The A0515 IC is used as an isolated DC power supply that provides the required isolated supply voltage for each power MOSFET.

5.5. Three-phase Five-level Diode-clamped Inverter (Power Circuit)

Three-phase Five-level Diode-clamped Inverter (Power Circuit) The three-phase inverter circuit along with its practical implementation is shown in Figure 5.11, where it shows three legs. Each leg represents one phase and it has eight power switches (power MOSFETs). The parameters of the power circuit are written in Table 5.2.

Table 5.2: Parameters of power circuit.

V_DC	Load impedance	Power MOSFET	Power diode
95V (each)	181.70+55.55jΩ	FQA24N60	VS-60APH03-N-S1

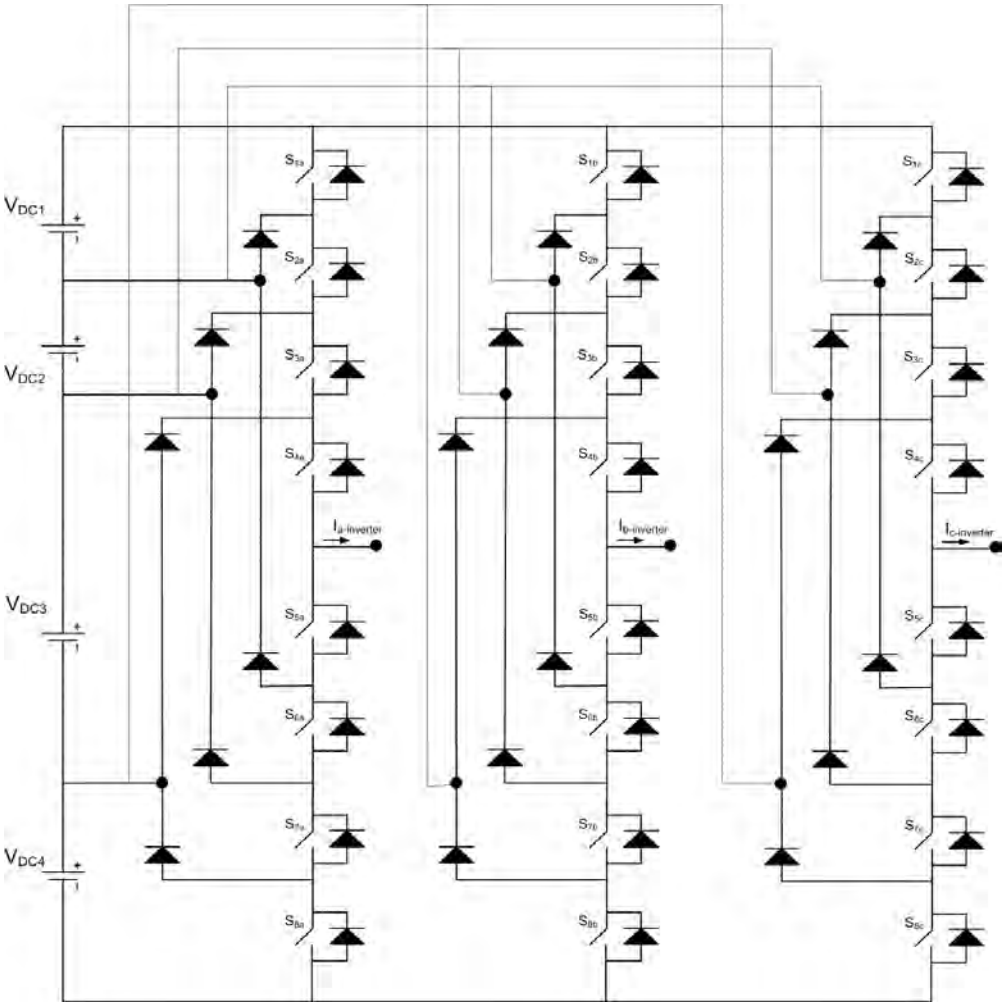

(a)

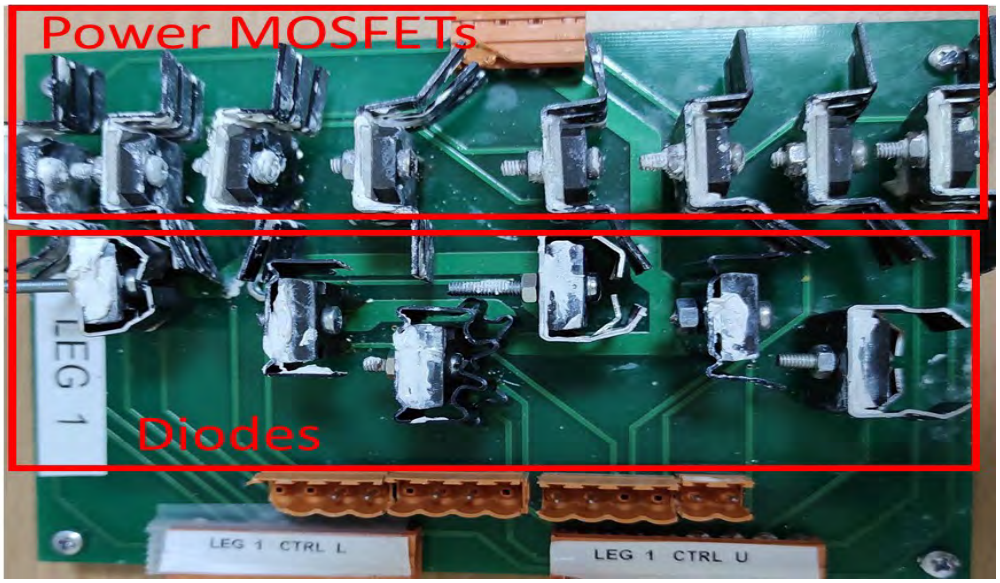

(b)

Figure 5.11: Topology of three-phase five-level diode-clamped inverter and its practical implementation, (a) circuit schematic, (b) its printed circuit.

5.6. Conclusion

Using two three-phase Five-level Diode-clamped Inverters with their control, carrier and drive circuits along with dSpase SCALEXIO as the control unit, the proposed microgrid is formed. The structure of the microgrid is shown in Figure 5.12. The dSpace contol unit is programmed using Matlab/Simulink, then it generates the control signals to both inverters that share the same load. The output of each inverter is filtered an measured and used as a feedback to the control unit.

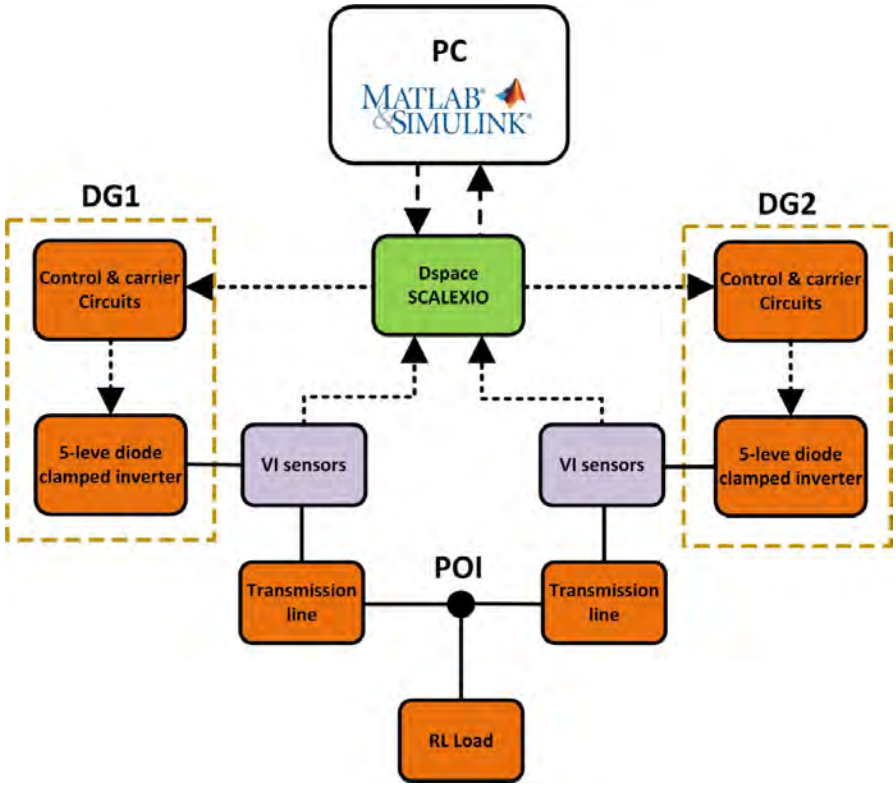

Figure 5.12: Block diagram of the microgrid understudy.

This chapter showed the structure of the five-level diode clamped inverter. The discussed structure for the inverter along with DSpace SCALEXIO Lab Box are used for both DGs that form the microgrid.

Chapter 6: Experimental Results

6.1. Introduction

This chapter shows the experimental results for the five-level diode clamped inverter and its control circuits. PI Virtual impedance droop control is also shown and discussed.

6.2. Experimental setup results

This section displays the experimental results for the experimental setup for the inverter and for all circuits from Figure 5.5 to Figure 5.11. The whole experimental setup is given in Figure 6.1.

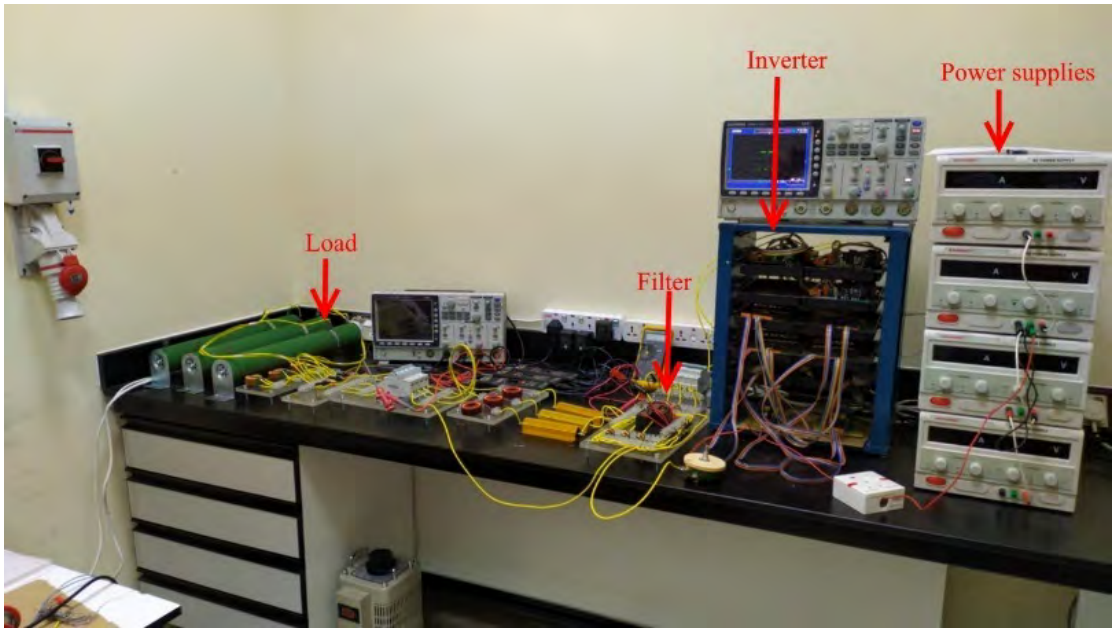

Figure 6.1: Experimental setup for the whole system.

6.2.1. Results of control and carrier circuits. Figure 6.2 portrays the practical result for the output of circuits from Figure 5.6 to Figure 5.10, which are the four carriers with amplitude of 500mV peak-to-peak each and shifted to cover the range from -1V to 1V with the frequency of 3.0 kHz.

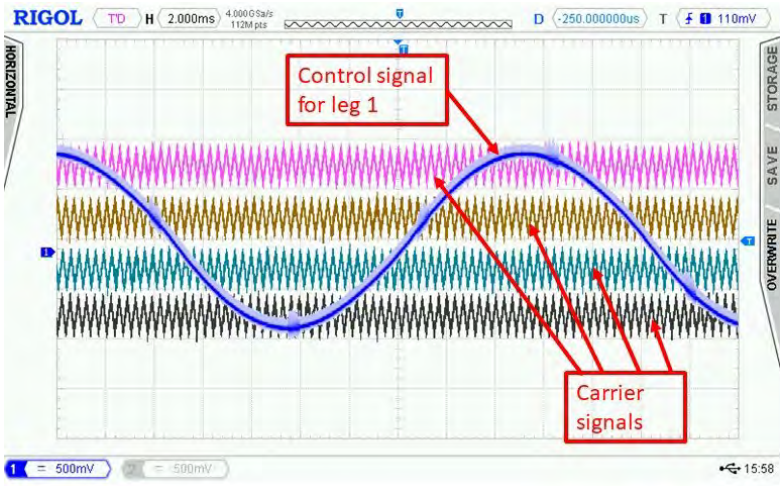

Figure 6.2: Experimental control signals of leg 1 with carrier signals

6.2.2. Results of dead-band and drive circuits. The waveforms of Figure 6.3 to Figure 6.5 show the experimental results for the comparator operation between the carrier and control signals. Figure 6.3 illustrates the output of the comparator circuit, which is the input of the dead-band circuit, shown in Figure 5.10, The experimental output of the dead-band circuit is shown in Figure 6.4 The result shows practical dead-band time T=13.3ns which closely matches the calculated one. The output of the dead-band circuit is used to operate the driver circuit of Figure 5.11. The experimental output signal and input signal of the driver circuit are shown in Figure 6.5.

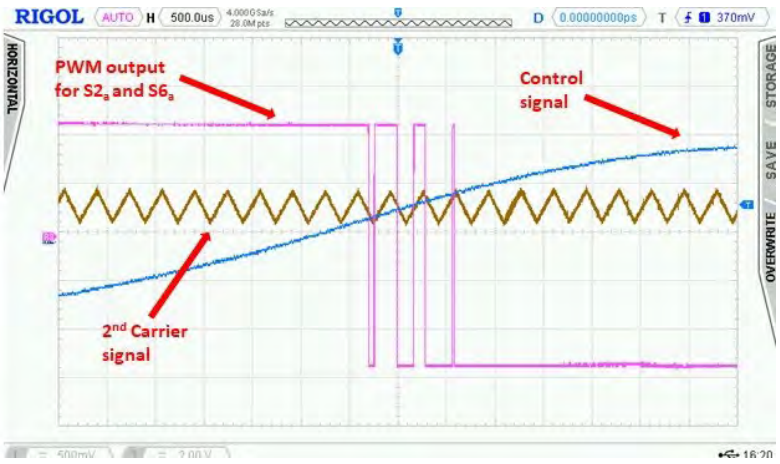

Figure 6.3: Experimental results for comparator output that will feed the PWM of switch S_{2a} and its compliment S_{6a}.

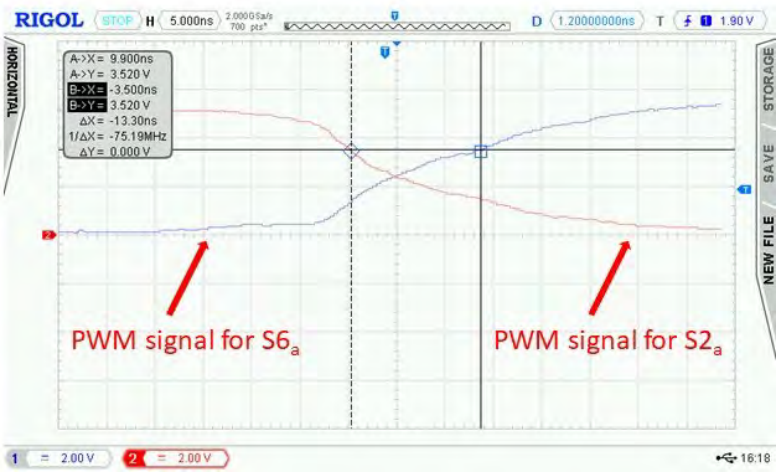

Figure 6.4: Experimental results for dead-band circuit output between S_{2a} and its compliment S_{6a}.

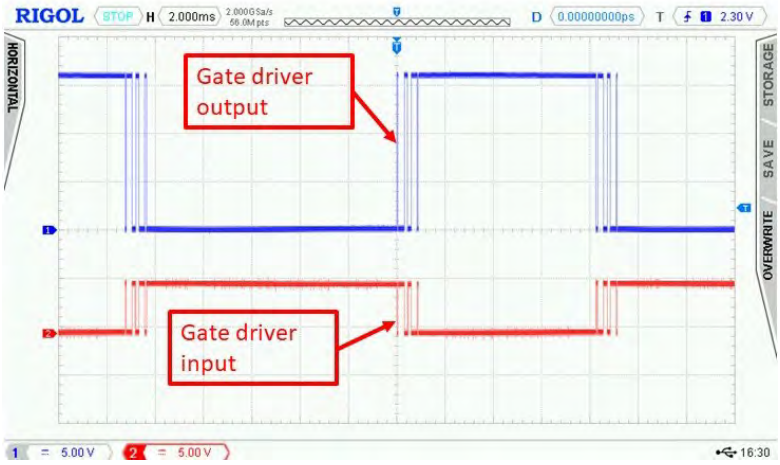

Figure 6.5: Experimental results for driving circuit for S_{2a} , channel 2 is the input and channel 1 is the output.

6.2.3. Results of power and filter circuits. The simulation result of the three-phase diode-clamped five-level inverter is shown in Figure 6.6-a (without filter) and its experimental result is shown in Figure 6.6-b. The voltage waveforms with the passive filter is depicted in Figure 6.7-a and in Figure 6.7-b for simulation and experimental results, respectively. The peak voltage for each phase is around 150V, which

yields 110 VRMS. Figure 6.8-a and Figure 6.8-b display the frequency spectrum of the output voltage for experimental setup without the filter and with the filter, respectively. While Figure 6.9-a and Figure 6.9-b depicts the output current with frequency spectrum without the filter and with the filter, respectively.

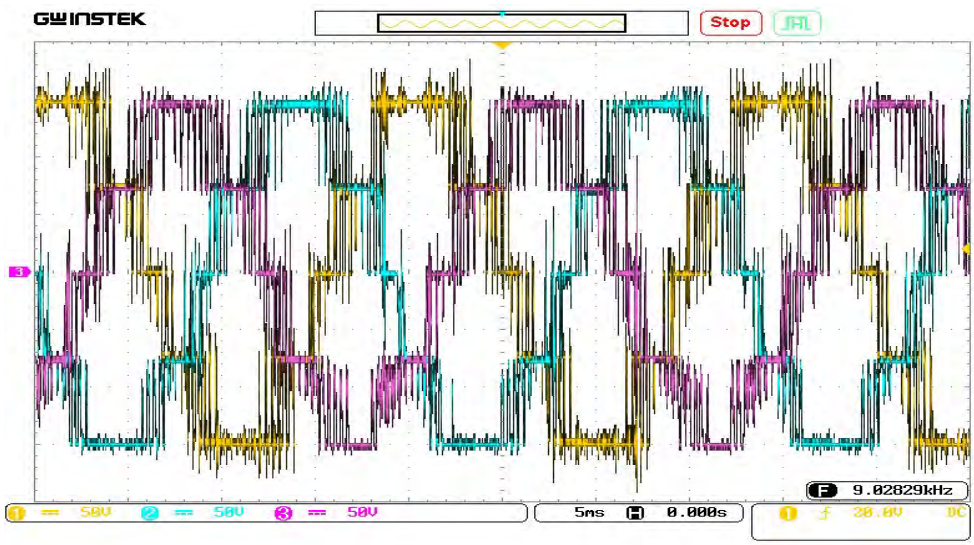

Figure 6.6: Inverter output waveforms from experimental setup without filter

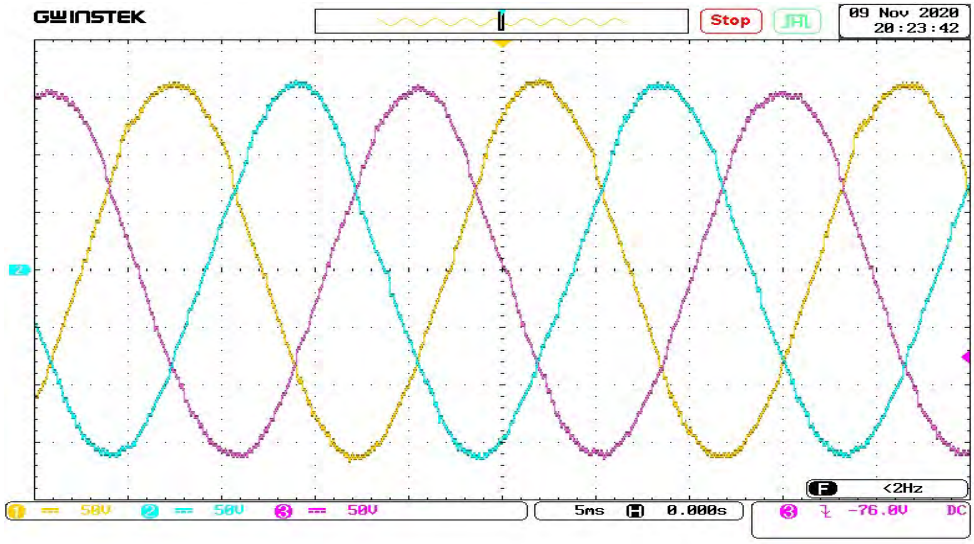

Figure 6.7: Inverter output waveforms from experimental setup after filter

(a)

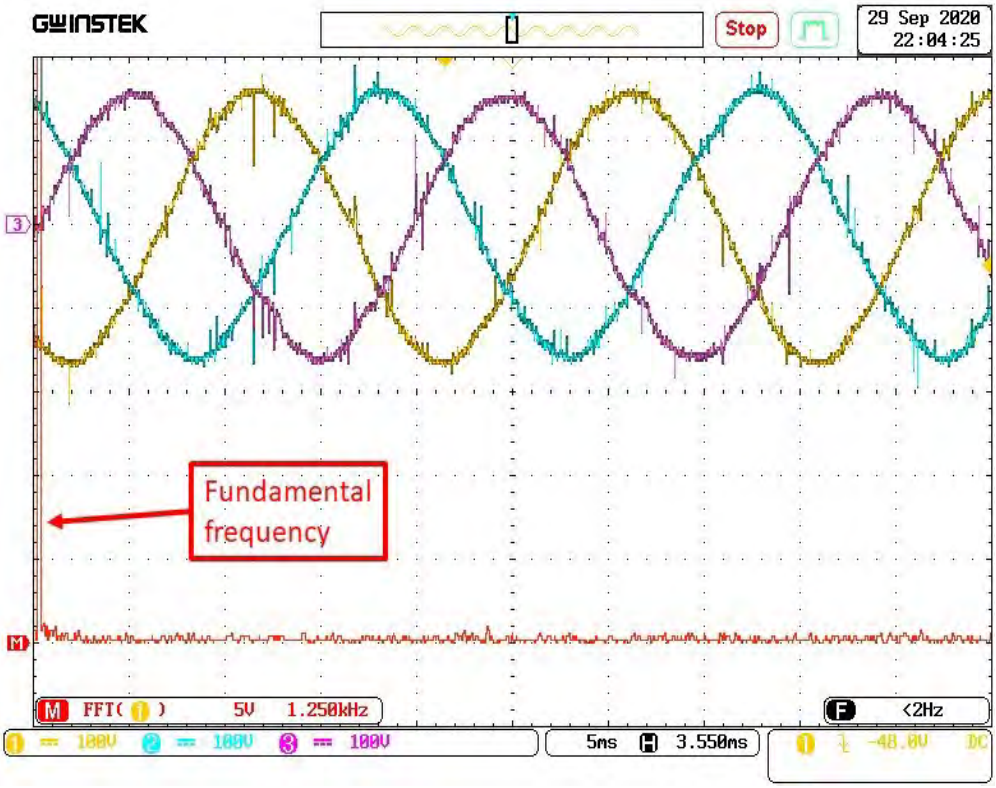

(b)

Figure 6.8: Experimental Frequency spectrum for output voltage with and without the filter, (a) without filter, (b) with adopted filter.

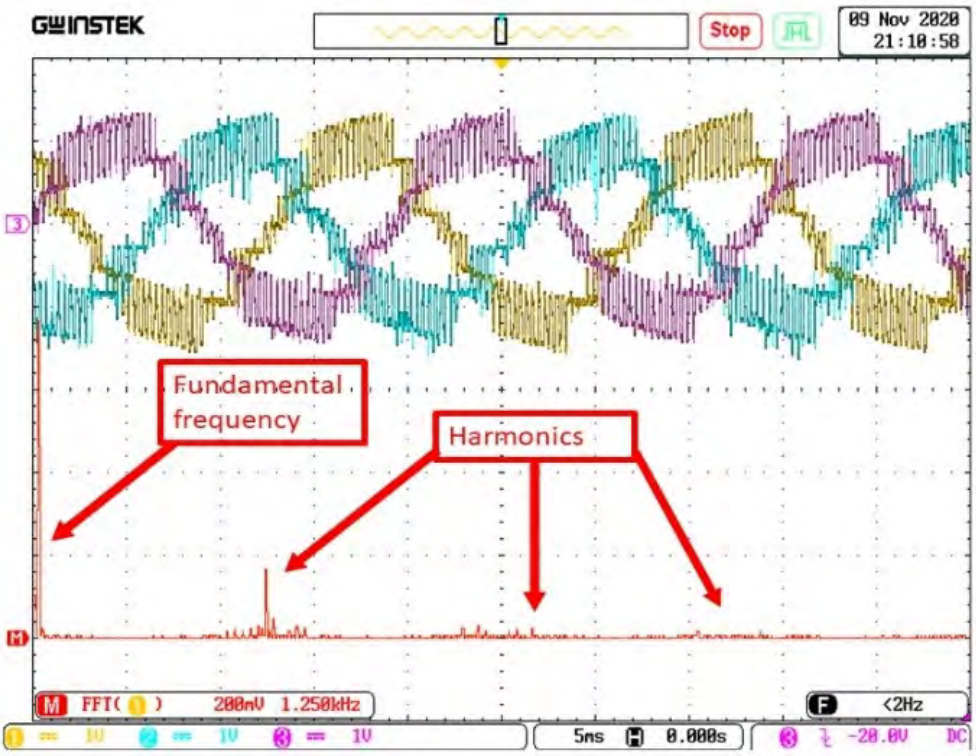

(a)

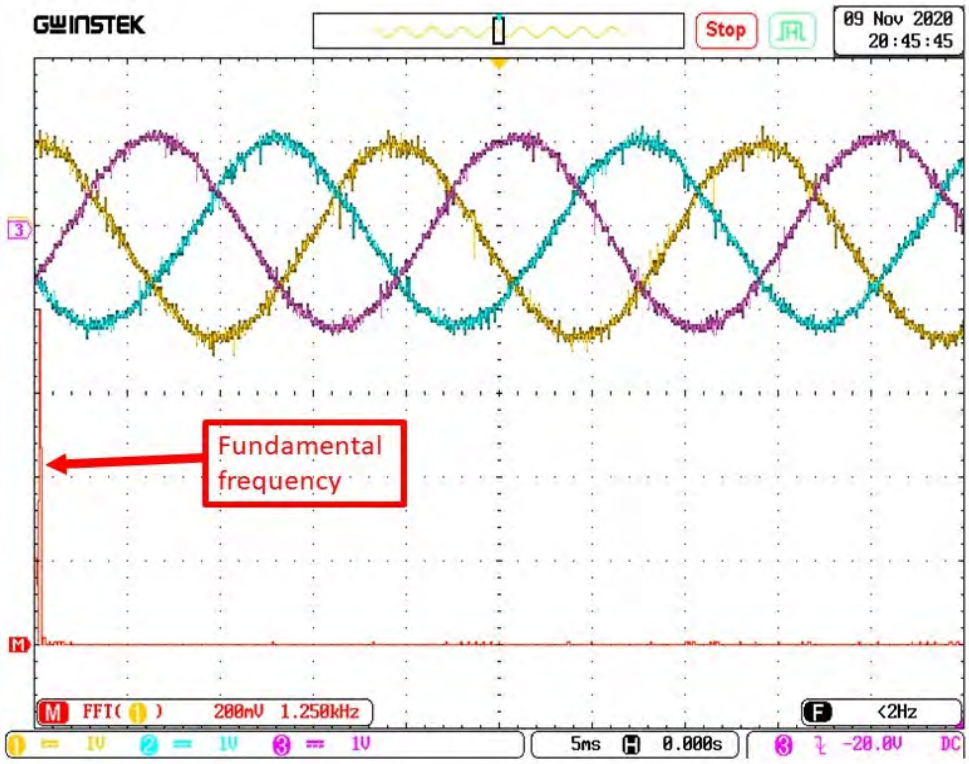

(b)

Figure 6.9: Experimental Frequency spectrum for the output current with and without the filter (scale :1V=1A), (a) without filter, (b) with filter.

6.3. PI Droop Results

The following figures shows initial results for virtual impedance droop control, applied on the microgrid built in chapter 5. The practical power sharing, active an reactive power, can be seen in fig 6.10.Moreover, the current and voltage stability of the system are shown in Figure 6.11 and Figure 6.12, respectively.

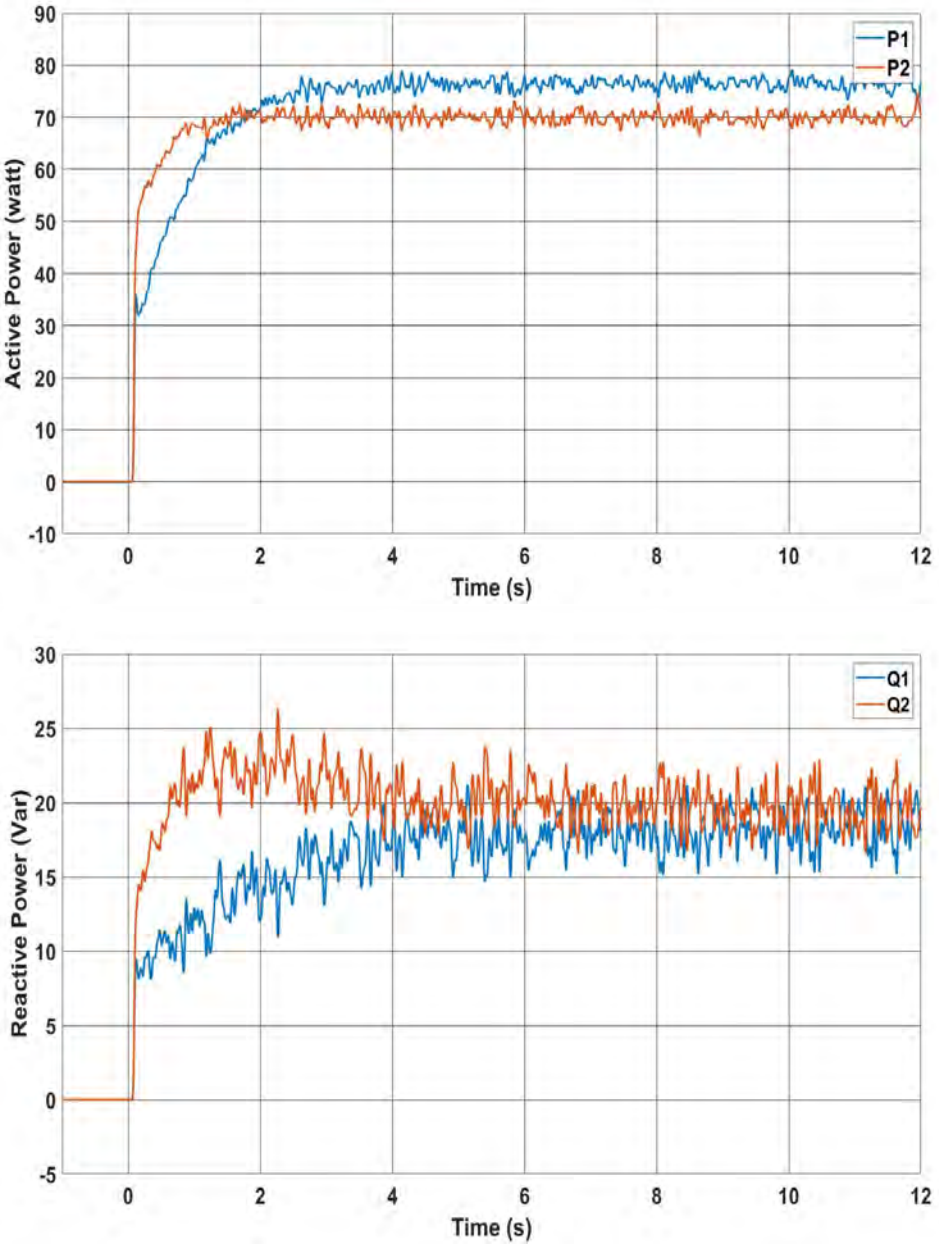

Figure 6.10: Practical active and reactive power sharing using VI droop control.

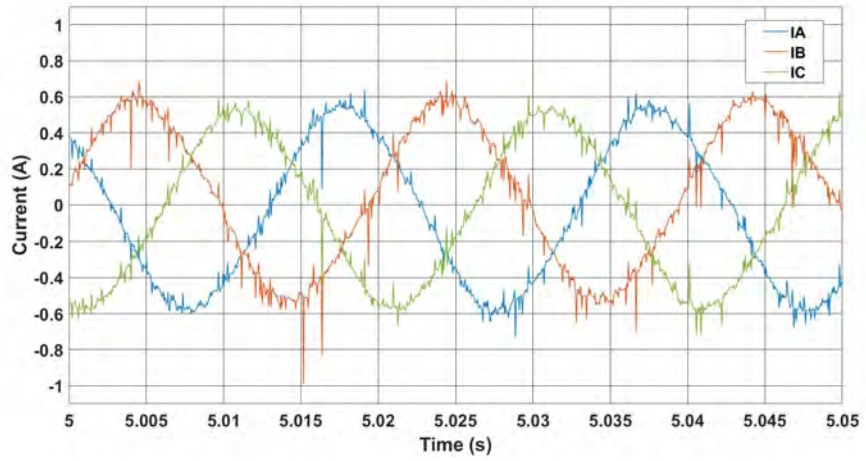

Figure 6.11: Practical active and reactive power sharing using VI droop control.

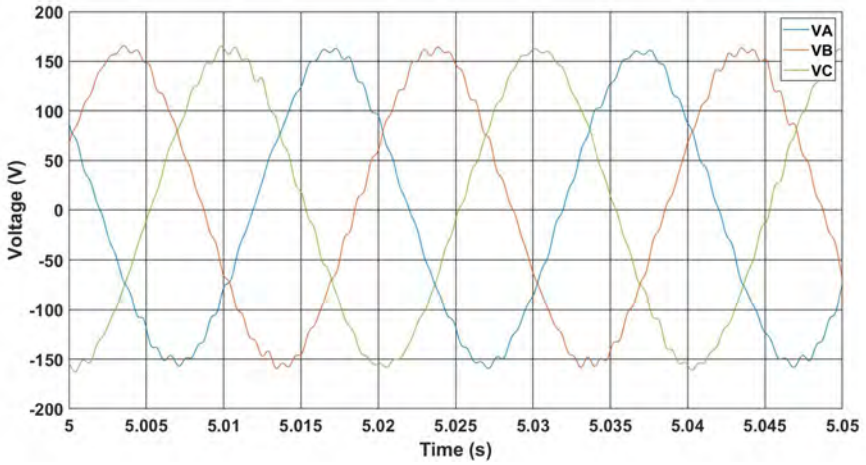

Figure 6.12: Practical active and reactive power sharing using VI droop control.

The feedback control used to get these results is PI control. These results show the setup's ability to be used for future research purposes.

6.4. Conclusion

The experimental results shows the stability of the built microgrid as well as its ability to manage the power sharing between DGs using PI virtual impedance droop control. The voltage and current ar also stable at the POI.

Chapter 7: Conclusion and Future Work

7.1. Findings and Conclusion

This thesis focused on designing and controlling of an AC microgrid in islanded mode. The microgrid consist of two diode clamped five-level inverter connected to a common load. Virtual impedance droop control, powered by two different feedback controllers, was adopted to operate the microgrid. The feedback controllers were state feedback and hyperbolic tangent SMC.

The simulation results showed the preponderance of both controllers compared to PI control, adaptive SMC, and power rate SMC. They also showed the superiority of State feedback control over hyperbolic tangent SMC in steady state operation while the hyperbolic tangent SMC a much faster mictogrid startup and smaller settling time compared to the state feedback controller.

The thesis also discussed the structure of the microgrid. Moreover both five level diode clamped three phase inverters circuits structure has been talked about in details. The provided experimental results showed the efficiency of and stability of both five level diode clamped inverters forming the microgrid. Additionally, preliminary experimental results for PI controller based virtual impedance droop control. The experimental results, taken using DSpace SCALILXIO real time controller, showed the ability of the practical microgrid to work efficiently and safely on other controllers.

7.2. Future Work

The future work after this thesis will focus on implementing the proposed controllers on the built microgrid, as well as developing and implementing more feedback controllers and study their performance on the same microgrid. Another novel multilevel inverter with reduced number of switches is being built to be connected to the microgrid.

References

[1] F. Ueda, K. Matsui, M. Asao, and K. Tsuboi, "Parallel-connections of pulsewidth modulated inverters using current sharing reactors," *IEEE Transactions on Power Electronics*, vol. 10, no. 6, pp. 673–679, 1995.

[2] T. Vandoorn, J. De Kooning, B. Meersman, and L. Vandevelde, "Review of primary control strategies for islanded microgrids with power-electronic interfaces," *Renewable and Sustainable Energy Reviews*, vol. 19, pp. 613–628, 2013.

[3] D. E. Olivares *et al.*, "Trends in microgrid control," *IEEE Transactions on Smart Grid*, vol. 5, no. 4, pp. 1905–1919, 2014.

[4] A. Alfergani, K. A. Alfaitori, A. Khalil, and N. Buaossa, "Control strategies in ac microgrid: A brief review," in *2018 9th International Renewable Energy Congress (IREC)*, 2018, pp. 1–6.

[5] B. Hartono, R. Setiabudy *et al.*, "Review of microgrid technology," in *2013 International Conference on QiR*, 2013, pp. 127–132.

[6] A. Llaria, O. Curea, J. Jiménez, and H. Camblong, "Survey on microgrids: unplanned islanding and related inverter control techniques," *Renewable energy*, vol. 36, no. 8, pp. 2052–2061, 2011.

[7] X. Zhou, T. Guo, and Y. Ma, "An overview on microgrid technology," in *2015 IEEE International Conference on Mechatronics and Automation (ICMA)*, 2015, pp. 76–81.

[8] P. Gaur and S. Singh, "Investigations on issues in microgrids," *Journal of Clean Energy Technologies*, vol. 5, no. 1, pp. 47–51, 2017.

[9] S. Parhizi, H. Lotfi, A. Khodaei, and S. Bahramirad, "State of the art in research on microgrids: A review," *IEEE Access*, vol. 3, pp. 890–925, 2015.

[10] A. Hirsch, Y. Parag, and J. Guerrero, "Microgrids: A review of technologies, key drivers, and outstanding issues," *Renewable and Sustainable Energy Reviews*, vol. 90, pp. 402–411, 2018.

[11] J. Banda and K. Siri, "Improved central-limit control for parallel-operation of dc-dc power converters," in *Proceedings of PESC'95-Power Electronics Specialist Conference*, vol. 2, 1995, pp. 1104–1110.

[12] J. Thunes, R. Kerkman, D. Schlegel, and T. Rowan, "Current regulator instabilities on parallel voltage-source inverters," *IEEE Transactions on Industry Applications*, vol. 35, no. 1, pp. 70–77, 1999.

[13] J. Yang, W. Yuan, Y. Sun, H. Han, X. Hou, and J. M. Guerrero, "A novel quasi-master-slave control frame for pv-storage independent microgrid," *International Journal of Electrical Power & Energy Systems*, vol. 97, pp. 262–274, 2018.

[14] D. Wu, F. Tang, T. Dragicevic, J. C. Vasquez, and J. M. Guerrero, "Coordinated primary and secondary control with frequency-bus-signaling for distributed generation and storage in islanded microgrids," in *IECON 2013-39th Annual Conference of the IEEE Industrial Electronics Society*, 2013, pp. 7140–7145.

[15] S. Wang, Z. Liu, J. Liu, R. An, and M. Xin, "Breaking the boundary: A droop and master-slave hybrid control strategy for parallel inverters in islanded microgrids," in *2017 IEEE Energy Conversion Congress and Exposition (ECCE)*, 2017, pp. 3345–3352.

[16] W.-C. Lee, T.-K. Lee, S.-H. Lee, K.-H. Kim, D.-S. Hyun, and I.-Y. Suh, "A master and slave control strategy for parallel operation of three-phase ups systems with different ratings," in *Nineteenth Annual IEEE Applied Power Electronics Conference and Exposition, 2004. APEC'04.*, vol. 1, 2004, pp. 456–462.

[17] X. Sun, L.-K. Wong, Y.-S. Lee, and D. Xu, "Design and analysis of an optimal controller for parallel multi-inverter systems," *IEEE Transactions on Circuits and Systems II: Express Briefs*, vol. 53, no. 1, pp. 56–61, 2006.

[18] X. Hou, Y. Sun, W. Yuan, H. Han, C. Zhong, and J. M. Guerrero, "Conventional p-ω/qv droop control in highly resistive line of low-voltage converter-based ac microgrid," *Energies*, vol. 9, no. 11, p. 943, 2016.

[19] A. Villalón, C. Muñoz, R. Aliaga, J. Muñoz, M. Rivera, and P. Zanchetta, "Power sharing control of islanded ac microgrid considering droop control and virtual impedance," in *2020 IEEE International Conference on Industrial Technology (ICIT)*, 2020, pp. 1139–1144.

[20] P. Monica and M. Kowsalya, "Control strategies of parallel operated inverters in renewable energy application: A review," *Renewable and Sustainable Energy Reviews*, vol. 65, pp. 885–901, 2016.

[21] Z. Liu, S. Ouyang, and W. Bao, "An improved droop control based on complex virtual impedance in medium voltage micro-grid," in *2013 IEEE PES Asia-Pacific Power and Energy Engineering Conference (APPEEC)*, 2013, pp. 1–6.

[22] J. He and Y. W. Li, "Analysis, design, and implementation of virtual impedance for power electronics interfaced distributed generation," *IEEE Transactions on Industry Applications*, vol. 47, no. 6, pp. 2525–2538, 2011.

[23] J. M. Guerrero, L. G. De Vicuna, J. Matas, M. Castilla, and J. Miret, "A wireless controller to enhance dynamic performance of parallel inverters in distributed generation systems," *IEEE Transactions on Power Electronics*, vol. 19, no. 5, pp. 1205–1213, 2004.

[24] P. Sreekumar and V. Khadkikar, "A new virtual harmonic impedance scheme for harmonic power sharing in an islanded microgrid," *IEEE Transactions on Power Delivery*, vol. 31, no. 3, pp. 936–945, 2015.

[25] H. Mahmood, D. Michaelson, and J. Jiang, "Accurate reactive power sharing in an islanded microgrid using adaptive virtual impedances," *IEEE Transactions on Power Electronics*, vol. 30, no. 3, pp. 1605–1617, 2014.

[26] J.-W. Kim, H.-S. Choi, and B. H. Cho, "A novel droop method for converter parallel operation," *IEEE Transactions on Power Electronics*, vol. 17, no. 1, pp. 25–32, 2002.

[27] S. Yang, C. Zhang, X. Zhang, R. Cao, and W. X. Shen, "Study on the control strategy for parallel operation of inverters based on adaptive droop method," in *2006 1ST IEEE Conference on Industrial Electronics and Applications*, 2006, pp. 1–5.

[28] W. Yao, M. Chen, M. Gao, and Z. Qian, "Development of communicationless hotswap paralleling for single-phase ups inverters based on adaptive droop method," in *2009 Twenty-Fourth Annual IEEE Applied Power Electronics Conference and Exposition*, 2009, pp. 1283–1287.

[29] K. O. Oureilidis and C. S. Demoulias, "A decentralized impedance-based adaptive droop method for power loss reduction in a converter-dominated islanded microgrid," *Sustainable Energy, Grids and Networks*, vol. 5, pp. 39–49, 2016.

[30] Q.-C. Zhong, "Robust droop controller for accurate proportional load sharing among inverters operated in parallel," *IEEE Transactions on Industrial Electronics*, vol. 60, no. 4, pp. 1281–1290, 2011.

[31] T. L. Vandoorn, B. Renders, L. Degroote, B. Meersman, and L. Vandevelde, "Active load control in islanded microgrids based on the grid voltage," *IEEE Transactions on Smart Grid*, vol. 2, no. 1, pp. 139–151, 2010.

[32] E. Tegling, M. Andreasson, J. W. Simpson-Porco, and H. Sandberg, "Improving performance of droop-controlled microgrids through distributed pi-control," in *2016 American Control Conference (ACC)*, 2016, pp. 2321–2327.

[33] J. Kim, J. M. Guerrero, P. Rodriguez, R. Teodorescu, and K. Nam, "Mode adaptive droop control with virtual output impedances for an inverter-based flexible ac microgrid," *IEEE Transactions on Power Electronics*, vol. 26, no. 3, pp. 689–701, 2010.

[34] J. C. Vasquez, J. M. Guerrero, A. Luna, P. Rodríguez, and R. Teodorescu, "Adaptive droop control applied to voltage-source inverters operating in grid-connected and islanded modes," *IEEE Transactions on Industrial Electronics*, vol. 56, no. 10, pp. 4088–4096, 2009.

[35] J. Matas, M. Castilla, L. G. De Vicuña, J. Miret, and J. C. Vasquez, "Virtual impedance loop for droop-controlled single-phase parallel inverters using a second-order general-integrator scheme," *IEEE Transactions on Power Electronics*, vol. 25, no. 12, pp. 2993–3002, 2010.

[36] C. Dou, Z. Zhang, D. Yue, and M. Song, "Improved droop control based on virtual impedance and virtual power source in low-voltage microgrid," *IET Generation, Transmission & Distribution*, vol. 11, no. 4, pp. 1046–1054, 2017.

[37] D. Gaonkar, J. M. Guerrero *et al.*, "Improved pf/qv and pv/qf droop controllers for parallel distributed generation inverters in ac microgrid," *Sustainable Cities and Society*, vol. 41, pp. 421–442, 2018.

[38] A. A. Kolesnikov, "Synergetic control theory," *Moscow, Energoatomizdat*, vol. 344, 1994.

[39] A. Kolesnikov, G. Veselov, A. Kolesnikov *et al.*, "Modern applied control theory: synergetic approach in control theory," *TRTU, Moscow, Taganrog*, pp. 4477–4479, 2000.

[40] S. Djennoune and M. Bettayeb, "Optimal synergetic control for fractional-order systems," *Automatica*, vol. 49, no. 7, pp. 2243–2249, 2013.

[41] A. V. Ojha and A. Khandelwal, "Control of non-linear system using backstepping," *International Journal of Research in Engineering and Technology*, vol. 4, no. 5, pp. 606–610, 2015.

[42] P. Kokotovic, "Joy of feedback: nonlinear and adaptive. bode prize lecture," in *Proc. of the 30th IEEE Conf. on Decision and Control*, 1991.

[43] B. Bossoufi, M. Karim, A. Lagrioui, M. Taoussi, and A. Derouich, "Observer backstepping control of dfig-generators for wind turbines variable-speed: Fpga-based implementation," *Renewable Energy*, vol. 81, pp. 903–917, 2015.

[44] Y. Fang, J. Fei, and Y. Yang, "Adaptive backstepping design of a microgyroscope," *Micromachines*, vol. 9, no. 7, p. 338, 2018.

[45] H. K. Khalil and J. W. Grizzle, *Nonlinear Systems*. Prentice hall Upper Saddle River, NJ, 2002, vol. 3.

[46] K. De Brabandere, B. Bolsens, J. Van den Keybus, A. Woyte, J. Driesen, and R. Belmans, "A voltage and frequency droop control method for parallel inverters," *IEEE Transactions on Power Electronics*, vol. 22, no. 4, pp. 1107–1115, 2007.

[47] R. Pérez-Ibacache, A. Yazdani, C. Silva, and J. C. Agüero, "Decentralized unified control for inverter-based ac microgrids subject to voltage constraints," *IEEE Access*, vol. 7, pp. 157 318–157 329, 2019.

[48] L. Fridman, "Technical committee on variable structure and sliding-mode control [technical activities]," *IEEE Control Systems Magazine*, vol. 36, no. 3, pp. 18–20, 2016.

[49] V. Utkin and H. Lee, "Chattering problem in sliding mode control systems," in *International Workshop on Variable Structure Systems, 2006. VSS'06.*, 2006, pp. 346–350.

[50] G. Song and R. Mukherjee, "A comparative study of conventional nonsmooth time-invariant and smooth time-varying robust compensators," *IEEE Transactions on Control Systems Technology*, vol. 6, no. 4, pp. 571–576, 1998.

[51] J. Y. Hung, W. Gao, and J. C. Hung, "Variable structure control: A survey," *IEEE Transactions on Industrial Electronics*, vol. 40, no. 1, pp. 2–22, 1993.

[52] C. J. Fallaha, M. Saad, H. Y. Kanaan, and K. Al-Haddad, "Sliding-mode robot control with exponential reaching law," *IEEE Transactions on Industrial Electronics*, vol. 58, no. 2, pp. 600–610, 2011.

[53] G. Bartolini, A. Pisano, E. Punta, and E. Usai, "A survey of applications of second-order sliding mode control to mechanical systems," *International Journal of Control*, vol. 76, no. 9-10, pp. 875–892, 2003.

[54] J. Rodriguez, J.-S. Lai, and F. Z. Peng, "Multilevel inverters: a survey of topologies, controls, and applications," *IEEE Transactions on Industrial Electronics*, vol. 49, no. 4, pp. 724–738, 2002.

[55] M. H. Rashid, *Power Electronics Handbook: Devices, Circuits and Applications*. Elsevier, 2010.

[56] M. Malinowski, K. Gopakumar, J. Rodriguez, and M. A. Perez, "A survey on cascaded multilevel inverters," *IEEE Transactions on Industrial Electronics*, vol. 57, no. 7, pp. 2197–2206, 2009.

[57] R. A. Krishna and L. P. Suresh, "A brief review on multi level inverter topologies," in *2016 International Conference on Circuit, Power and Computing Technologies (ICCPCT)*, 2016, pp. 1–6.

[58] I. Colak, E. Kabalci, and R. Bayindir, "Review of multilevel voltage source inverter topologies and control schemes," *Energy Conversion and Management*, vol. 52, no. 2, pp. 1114–1128, 2011.

[59] N. Mohan, W. P. Robbins, and T. Undeland, "Power electronics: Converters, applications and design," 2003.

[60] S. P. Sunddararaj, S. Srinivasarangan Rangarajan *et al.*, "An extensive review of multilevel inverters based on their multifaceted structural configuration, triggering methods and applications," *Electronics*, vol. 9, no. 3, p. 433, 2020.

[61] V. K. Kanike and S. Raju, "Analysis of switching sequence operation for reduced switch multilevel inverter with various pulse width modulation methods," *Frontiers in Energy Research*, vol. 7, p. 164, 2020.

[62] R. Gupta, A. Ghosh, and A. Joshi, "Switching characterization of cascaded multilevel-inverter-controlled systems," *IEEE Transactions on Industrial Electronics*, vol. 55, no. 3, pp. 1047–1058, 2008.

[63] P. Bhagyalakshmi, B. M. Varghese, and B. M. Jos, "Switched capacitor multilevel inverter with different modulation techniques," in *2017 International Conference on Innovations in Information, Embedded and Communication Systems (ICIIECS)*, 2017, pp. 1–6.

[64] A. Elnady and M. Suleiman, "Simulation and experimental comparison between multilevel and conventional inverters," *International Journal of Power and Energy Systems*, vol. 37, no. 3, 2017.

[65] Z. Jinghua and L. Zhengxi, "Research on hybrid modulation strategies based on general hybrid topology of multilevel inverter," in *2008 International Symposium on Power Electronics, Electrical Drives, Automation and Motion*, 2008, pp. 784–788.

[66] M. Esa and J. Muralidhar, "Common mode voltage reduction in diode clamped mli using phase disposition spwm technique," in *2018 4th International Conference on Electrical Energy Systems (ICEES)*, 2018, pp. 279–289.

[67] V. Priya, M. Maheswari, and R. Saranya, "Dvr using diode clamped multilevel inverter with phase disposition pulse width modulation technique," *International Journal of Computer Applications*, vol. 71, no. 15, 2013.

[68] Y. Cheng, C. Qian, M. L. Crow, S. Pekarek, and S. Atcitty, "A comparison of diode-clamped and cascaded multilevel converters for a statcom with energy storage," *IEEE Transactions on Industrial Electronics*, vol. 53, no. 5, pp. 1512–1521, 2006.

[69] Y. Cheng and M. L. Crow, "A diode-clamped multi-level inverter for the statcom/bess," in *2002 IEEE Power Engineering Society Winter Meeting. Conference Proceedings (Cat. No. 02CH37309)*, vol. 1, 2002, pp. 470–475.

[70] A. B. Sankar and R. Seyezhai, "Investigation of pmsg fed diode-clamped multilevel inverter for wind energy system," in *Advanced Materials Research*, vol. 768. Trans Tech Publ, 2013, pp. 16–22.

[71] M. T. Hamayun, C. Edwards, H. Alwi *et al.*, *Fault tolerant control schemes using integral sliding modes*. Springer, 2016.

[72] R. L. Boylestad, *Electronic devices and circuit theory*. Pearson Education India, 2009.

[73] M. M. Siam, B. Williams, and S. Finney, "Improved active power filter with triplen deadband pwm," in *PESC Record. 27th Annual IEEE Power Electronics Specialists Conference*, vol. 2, 1996, pp. 1899–1905.

Vita

Mohammad Saad Suleiman was born in 1991, in Jordan. He moved to United Arab Emirates in 2001. He graduated from AL-Shola private school in 2009. He received a bachelor of Sciences in Electrical and Electronics Engineering from the University of Sharjah in 2014. Currently, he is working as a laboratory engineer at the University of Sharjah and is doing a master of Sciences in Electrical Engineering at American University of Sharjah. His research interests are power electronics, renewable energy systems and their controls.